Electronic circular dichroism spectra using the algebraic diagrammatic construction schemes of the polarization propagator up to third order

Scott, Mikael; Rehn, Dirk R.; Coriani, Sonia; Norman, Patrick; Dreuw, Andreas

Published in:
Journal of Chemical Physics

Link to article, DOI:
10.1063/5.0038315

Publication date:
2021

Document Version
Peer reviewed version

The Journal of Chemical Physics

Electronic circular dichroism spectra using the algebraic diagrammatic construction schemes of the polarization propagator up to third order

Mikael Scott,[1] Dirk R. Rehn,[1] Sonia Coriani,[2] Patrick Norman,[3] and Andreas Dreuw*[1, a)]
[1)] *Interdisciplinary Center for Scientific Computing, Ruprecht-Karls University, Im Neuenheimer Feld 205, 69120 Heidelberg, Germany*
[2)] *DTU Chemistry, Technical University of Denmark, Kemitorvet Bldg 207, DK-2800 Kongens Lyngby, Denmark*
[3)] *Department of Theoretical Chemistry and Biology, School of Engineering Sciences in Chemistry, Biotechnology and Health, KTH Royal Institute of Technology, SE-106 91 Stockholm, Sweden*

(Dated: 14 January 2021)

Expressions for the calculation of rotatory strengths using the algebraic diagrammatic construction (ADC) scheme of the polarization propagator in both length and velocity gauges have been implemented. This enables the simulation of electronic circular dichroism (ECD) spectra at the ADC level up to third order of perturbation theory. The ADC(n) methods produce rotatory strengths of comparable accuracy to those obtained with coupled cluster methods of corresponding approximation levels as evaluated for methyloxirane, methylthiirane, dimethyloxirane, dimethylthiirane, hydrogen peroxide and dihydrogen disulfide. ECD spectra of (1R)-camphor, (1R)-norcamphor and (1R)-fenchone computed at the third order ADC(3) level of theory are shown to agree very favorably with experimental gas phase spectra demonstrating the usefulness of ADC for the calculation of chiro-optical properties of organic molecules. ADC(2) in combination with the polarizable continuum model (PCM) is shown to successfully reproduce the ECD spectrum of the L-epinephrine enantiomer in water, further demonstrating the applicability of this approach.

I. INTRODUCTION

Electronic circular dichroism (ECD) is a widely used linear optical effect to gain information about the stereochemistry of molecular systems.[1] Different enantiomers of a chiral molecule preferentially interact with one of the two circularly polarized components of plane polarized light. This results in a rotation of the plane of polarization, as observed in optical rotation measurements, and differential absorption, as detected by ECD spectroscopy. As a spectroscopic tool, ECD has found use in a wide range of scientific fields ranging from biochemistry where it is commonly employed to detect the secondary structures of proteins[2] to pharmaceutical synthesis where enantiomeric purity is of importance.[3] Especially important in ECD spectroscopy is the sign of the measured signal as enantiomers produce mirror-like ECD spectra. This allows for quick and straightforward quality control of synthesized chiral molecules once accurate theoretical predictions have been carried out. Furthermore, achiral systems interacting with chiral systems, e.g. a solvent arranging itself around a solute in a structurally chiral manner, can give rise to a CD signal which is a process referred to as induced circular dichroism (ICD). Thus ICD provides information not only of the absolute configuration of the chiral system but also of the orientation of its achiral (e.g. solvent) counterpart.[4]

For the prediction of ECD spectra many theoretical methods have been developed over the last decades with methods suited for different molecular sizes and environments. Progress has been made and highly accurate ECD spectra can be simulated and compared directly with experiment.[1] For proteins and macro molecules semi-empirical methods have been shown to accurately reproduce ECD spectra of low-lying excitations.[5,6] Similarly, for molecules on the order of hundreds of atoms, time-dependent Hartree-Fock (TD-HF)[7–9] and time-dependent Density Functional Theory (TD-DFT)[10–14] have proven successful. For ECD spectra of small chiral molecules, on the order of tens of electrons, configuration interaction (CI)[15] and linear response based on a complete active space self-consistent field (CAS-SCF) reference[16] can be applied. Furthermore, the well-known equation of motion coupled cluster (EOM-CC)[17,18] and the similar linear response coupled cluster (CCLR) approach[19–22] have been applied to the calculation of ECD spectra and proven to be highly accurate.

The algebraic diagrammatic construction (ADC)[23] scheme for the polarization propagator is an *ab initio* method which shares many features with CC excited-state methods. ADC requires the solution of an Hermitian eigenvalue equation, and provides a hierarchy of approximations. In comparison with CC methods, this has the advantage of not requiring the solution of both a left and right-hand side equation. It has been employed to predict several linear and non-linear properties, e.g., two-photon absorption (TPA)[24] and resonant inelastic x-ray scattering (RIXS).[25] Further, static properties such as static polarizabilities and C_6 dispersion coefficients[26,27] have recently been investigated. The computational effort required for ADC(n) schemes scales as n^4 for ADC(1), n^5 for ADC(2), n^6 for ADC(2)-x and

[a)] Electronic mail: dreuw@uni-heidelberg.de

ADC(3/2), with n being the number of basis functions. For comparison, the corresponding CC schemes CC2, EOM-CCSD and CC3 formally scale as n^5, n^6 and n^7, respectively, however, require the solution for the corresponding ground state as well.

Here, we report the first implementation of ADC-based methods to simulate chiro-optical properties such as ECD.

We choose methyloxirane and methylthiirane molecules as well as their dimethylated derivatives to investigate the performance of the ADC methods in the calculation of ECD spectra. For these molecules, highly resolved gas phase spectra exist for comparison. Furthermore, we include the inherently chiral hydrogen peroxide H_2O_2 and dihydrogen disulfide H_2S_2 for their small size and well studied chiro-optical properties. Beside these relatively small molecules, we evaluate the ECD spectra of camphor, norcamphor and fenchone using a third order ADC scheme in comparison with experimental gas phase spectra.[28–32] The latter molecules have previously been investigated using TD-DFT but not yet using a third order *ab initio* method. We also include epinephrine, a common medical drug and hormone,[33] for which there are aqueous ECD solution spectra reported.[34] The molecular structures of the investigated systems are shown in Fig. 1.

A complication in the calculation of ECD spectra is the lack of gauge invariance of approximate solutions of the Schrödinger equation which can lead to origin dependent rotatory strengths in the length gauge. This is circumvented in one of two ways: (i) using magnetic-field dependent "gauge-including" atomic orbitals (GIAOs, also referred to as London orbitals);[11,35–42] or alternatively (ii) by a gauge transformation to the velocity gauge which is formally origin invariant.[19,43–47] The latter strategy is referred to as velocity gauge formalism or gradient form of the rotatory strength, and this method will be used throughout this work. For sake of completeness, the length gauge formulation of the rotatory strength is also briefly presented.

Experimentally,an ECD spectrum is recorded by measuring the difference in absorption between left and right circularly polarized light,

$$\Delta\epsilon(\omega) = \epsilon_L(\omega) - \epsilon_R(\omega), \tag{1}$$

where $\epsilon_L(\omega)$ and $\epsilon_R(\omega)$ are the absorption coefficients, at incident frequency ω, for left and right circularly polarized light, respectively. The measured signal may then be related to the underlying rotatory strength governing the excitation by integration over a frequency range $[\omega_1, \omega_2]$,[48] as

$$R = 22.97 \times \int_{\omega_1}^{\omega_2} \frac{\Delta\epsilon(\omega)}{\omega} d\omega, \tag{2}$$

where the photon energy ω is in eV and $\Delta\epsilon(\omega)$ is given in L mol^{-1} cm^{-1}. The rotatory strength, R, is in the usually reported units of 10^{-40} esu $\cdot$ cm $\cdot$ erg/G or 10^{-40} c.g.s. units.[49] The crucial assumption of Eq. (2) is that the integrated peak results from one electronic transition only. This is not necessarily the case and not known *a priori*, which emphasizes the need for robust theoretical models assisting in the interpretation of the experimental ECD spectra.

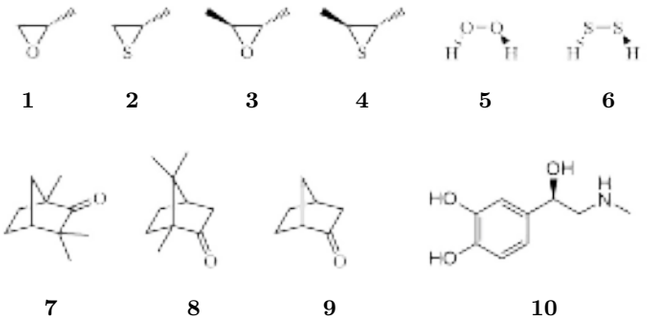

FIG. 1. **1** (R)-methyloxirane, **2** (R)-methylthiirane, **3** (R,R)-dimethyloxirane, **4** (R,R)-dimethylthiirane, **5** hydrogen peroxide, **6** hydrogen persulfide, **7** (1R)-camphor, **8** (1R)-fenchone, **9** (1R)-norcamphor and **10** L-epinephrine.

II. THEORY AND METHODOLOGY

A. Optical rotatory and oscillator strengths in the length- and velocity-gauge formalism within the intermediate state representation

The fundamental property governing the preferential absorption of circularly polarized light is the rotatory strength, R_{n0}. It is given by the well-kown Rosenfeld equation[50] as the scalar product of the electric and magnetic transition dipole moments between the ground state $|\Psi_0\rangle$ and an excited state $|\Psi_n\rangle$,

$$R_{n0} = \mathrm{Im}\,\langle\Psi_0|\,\hat{\boldsymbol{\mu}}\,|\Psi_n\rangle \cdot \langle\Psi_n|\,\hat{\mathbf{m}}\,|\Psi_0\rangle\,, \tag{3}$$

where $\hat{\boldsymbol{\mu}}$ and $\hat{\mathbf{m}}$ are the electric and magnetic dipole operators, respectively. From the Rosenfeld equation, we can see that the electric transition dipole moment and the magnetic transition dipole moment must be non-orthogonal for a transition to be active in ECD. Using the electric dipole operator, $\hat{\boldsymbol{\mu}} = -e\hat{\boldsymbol{r}}$, and the magnetic dipole operator, $\hat{\mathbf{m}} = \frac{ie\hbar}{2m_e c}\hat{\boldsymbol{r}} \times \hat{\boldsymbol{\nabla}}$,[43] within Eq. (3) yields the rotatory strength in its *length gauge* formulation,

$$R^{\boldsymbol{r}}_{n0} = -\frac{e^2\hbar}{2m_e c}\,\langle\Psi_0|\,\hat{\boldsymbol{r}}\,|\Psi_n\rangle \cdot \langle\Psi_n|\,\hat{\boldsymbol{r}} \times \hat{\boldsymbol{\nabla}}\,|\Psi_0\rangle\,, \tag{4}$$

where e is the elementary charge, m_e is the electron mass, c is the speed of light and $\hbar$ is the reduced Planck constant. In the sum-over-states expression this form of the rotatory strength sums up to zero, which results in zero rotatory strengths far away from resonance,[51] but lacks

gauge-origin independence.[52] Hence, a translation of the origin of the position operator alters the calculated rotatory strength. As mentioned previously, we circumvent the origin dependence of the rotatory strengths in the length gauge by employing the velocity gauge. By using the fact that the position operator commutes with every term in the electronic molecular Hamiltonian, except the kinetic energy operator,[47,53]

$$\frac{\hbar^2}{m}\langle n|\,\hat{\boldsymbol{\nabla}}\,|f\rangle = \langle n|\,[\hat{\boldsymbol{r}},\hat{\boldsymbol{H}}]\,|f\rangle = \hbar\omega_{fn}\,\langle n|\,\hat{\boldsymbol{r}}\,|f\rangle\,, \tag{5}$$

and applying this to Eq. (4) yields the rotatory strength in the velocity (gradient) form,

$$R^{\boldsymbol{\nabla}}_{n0} = -\frac{e^2\hbar^2}{2m_e^2c}\cdot\frac{1}{\omega_{n0}}\,\langle\Psi_0|\,\hat{\boldsymbol{\nabla}}\,|\Psi_n\rangle\cdot\langle\Psi_n|\,\hat{\boldsymbol{r}}\times\hat{\boldsymbol{\nabla}}\,|\Psi_0\rangle\,. \tag{6}$$

The corresponding oscillator strength of the same transition is computed in the length gauge as[43]

$$f^{\boldsymbol{r}}_{n0} = \frac{2m_e\omega_{n0}}{3\hbar}\,|\langle\Psi_0|\,\hat{\boldsymbol{r}}\,|\Psi_n\rangle|^2\,, \tag{7}$$

which in analogy to the rotatory strength can be transformed to yield the oscillator strength in the velocity gauge

$$f^{\boldsymbol{\nabla}}_{n0} = \frac{2\hbar}{3m_e\omega_{n0}}\left|\langle\Psi_0|\,\hat{\boldsymbol{\nabla}}\,|\Psi_n\rangle\right|^2. \tag{8}$$

The two forms of the oscillator strength are origin independent and they are usually computed together as a measure of basis completeness.

In the context of the algebraic diagrammatic construction scheme for the polarization propagator, the excitation energies and transition moments required in order to evaluate Eq. (6) are obtained by finding the eigenvectors and eigenvalues of the Hermitian ADC matrix $\mathbf{M}$, which is a representation of the electronic Hamiltonian $\hat{H}$ in so-called intermediate states $|\tilde{\Psi}_I\rangle$ shifted by the exact ground-state energy, E_0.[54,55] The ADC matrix is connected to the diagonal representation of the shifted Hamiltonian in exact states

$$\Omega_{nm} = \delta_{nm}\hbar\omega_n = \langle\Psi_n|\,\hat{H} - E_0\,|\Psi_n\rangle\,, \tag{9}$$

by unitary transformation

$$\mathbf{M} = \mathbf{X}\boldsymbol{\Omega}\mathbf{X}^\dagger, \tag{10}$$

with the eigenvector matrix $\mathbf{X}$. Ground-to-excited state transition moments for a given operator $\hat{O}$ can be evaluated by contracting an eigenvector $\mathbf{x}^n$ with the vector of so-called modified transition moments $\mathbf{F}(\hat{O})$

$$\langle\Psi_0|\,\hat{O}\,|\Psi_n\rangle = \mathbf{x}^n\mathbf{F}^\dagger(\hat{O}), \tag{11}$$

which correspond to the transition moments between the ground state and the intermediate states

$$F_I(\hat{O}) = \langle\Psi_0|\,\hat{O}\,|\tilde{\Psi}_I\rangle\,. \tag{12}$$

To efficiently evaluate transition moments for different operators, the modified transition moments are not constructed explicitly but rather the transition density $\boldsymbol{\rho}^{0n}$ is calculated

$$\rho^{0n}_{pq} = \langle\Psi_0|\,c_p^\dagger c_q\,|\Psi_n\rangle = \sum_I x_I^n\,\langle\Psi_0|\,c_p^\dagger c_q\,|\tilde{\Psi}_I\rangle\ , \tag{13}$$

where $c_p^\dagger$ and c_q are creation and annihilation operators in second quantization. The transition moments are then evaluated as

$$\langle\Psi_0|\,\hat{O}\,|\Psi_n\rangle = \sum_{pq}\rho^{0n}_{pq}o_{pq}, \tag{14}$$

with the property integrals $o_{pq} = \langle\phi_p|\,\hat{O}\,|\phi_q\rangle$ in the molecular orbital basis $\{\phi_p\}$. By consistently constructing the intermediate states up to a given order n of perturbation theory using the Møller-Plesset Hamiltonian partitioning one arrives at the corresponding ADC(n) scheme. Using the eigenvalues and eigenvectors of the third-order ADC matrix with the second-order modified transition moments is referred to as ADC(3/2). This mixed third and second order scheme is used throughout this paper and called ADC(3) for brevity.[56,57]

Full-ADC is formally gauge invariant. However, this is not true for truncated ADC schemes. The remaining difference between the length and velocity forms of the oscillator and rotatory strengths occurs in the highest-order contributions of their perturbational expansion, in other words in $\mathcal{O}^{(n)}$ for ADC(n). Consequently, the gauge-variance of ADC(3/2) is of the same order as ADC(2), i.e. the differences occur in the $\mathcal{O}^{(2)}$ contributions. For further theoretical details regarding the length-velocity gauge behaviour of ADC(n) methods, see Ref. 58.

B. Computational details

To simulate the ECD spectra, the computed rotatory strengths are converted from a.u. to 10^{-40} c.g.s. using the conversion factor 471.44 and subsequently broadened by a Lorentzian function,

$$\Delta\epsilon(\omega) = \sum_n \Delta\epsilon_n\frac{\gamma_n}{(\omega-\omega_{n0})^2+\gamma_n^2} \tag{15}$$

$$\Delta\epsilon_n = \frac{\omega R_{n0}}{22.94\pi}\times 10^{40}, \tag{16}$$

where $\Delta\epsilon_n$ is the peak intensity of the n-th transition given in L mol $^{-1}$ cm^{-1}, R_{n0} is the rotatory strength in 10^{-40} c.g.s., γ_n is the Lorentzian broadening factor, ω and ω_{n0} are the incident optical frequency and excitation energy in eV. A broadening factor corresponding to full width at half maximum of $\gamma_n = 1000$ cm^{-1} is used throughout this work.[59]

Calculations of oscillator and rotatory strengths in both length and velocity gauges using ADC were performed using a development version of Q-Chem 5.2.[60]

For the CC calculations of the same properties, Dalton2018 was used.[61] Dunning basis sets were employed throughout the paper.[62–65] The origin for the position operator was set to the hetero atom for the oxiranes, thiiranes and camphor and its derivatives and to one of the oxygen/sulfur atoms in the symmetrical H_2O_2 and H_2S_2 molecules. Geometries of methyloxirane, dimethyloxirane, methylthiirane and dimethylthiirane were optimized using MP2/aug-cc-pVTZ and those of H_2O_2 and H_2S_2 at MP2/d-aug-cc-pVTZ level. For camphor, norcamphor and fenchone, DFT/CAM-B3LYP[66] and aug-cc-pVTZ were used for the geometry optimization.

III. RESULTS AND DISCUSSION

A. ECD spectra of Methyloxirane and Methylthiirane

Methyloxirane has been widely used for the evaluation of quantum chemical methods for the simulation of ECD spectroscopy, primarily due to its small size as well as its available gas phase circular dichroism spectrum.[67,68] Furthermore, there is extensive literature available, both experimental and theoretical work, covering electronic structure,[69] excited state properties,[70] and two-photon absorption ECD.[71] CC methods have proven successful in reproducing the gas phase ECD spectrum.[72] Inclusion of molecular dynamics have addressed the water solution spectrum[73] and use of a polarizable embedding model have also addressed the spectrum in various solvents.[74–76]

It has been shown that inclusion of diffuse functions is important to ensure correct signs of the optical rotatory strength of methyloxirane.[77] Pople basis sets seem inadequate even with diffuse functions, while Dunning basis sets have proven more capable.[11] Therefore, we performed an extensive basis set study for ADC(2), ADC(3), CC2 and CCSD using Dunning basis sets and comparing to experimentally measured values of methyloxirane. The excitation energies, oscillator and rotatory strengths calculated at the ADC(2), ADC(3), CC2 and CCSD levels of theory for the nine lowest excited states of (*R*)-methyloxirane and (*R*)-methylthiirane are collected in Table I (see Table S1-S4 in the supporting information for all excited states computed). The simulated ECD and UV/VIS spectra at the same levels of theory of the 15 energetically lowest excited states are shown in Fig. 2.

Basis set impact on methyloxirane. Starting with ADC(2) and CC2, the smallest basis of the cc-pVXZ series (X: D,T,Q), cc-pVDZ, yields nearly identical excitation energies for ADC(2) and CC2, with the first vertically excited state calculated at 8.24 eV at ADC(2) and 8.35 eV at CC2 level, which should be compared with the experimental value of 7.08 eV.[67] Increasing the basis set size from double to quadruple-zeta lowers the excitation energy to 7.51 eV and 7.54 eV for ADC(2) and CC2, respectively. However, the rotatory strength of the first transition is largely unaffected and is roughly overestimated by a factor of two compared to experiment. However, the reported value in Ref. 67 is based on Eq. (2) with the limits of integration determined by a low-level CI calculation possibly impairing the analysis. In general, careful analysis is always needed when comparing computed and experimental rotatory strength.

Turning to the singly-augmented, aug-cc-pVXZ series (X: D,T), aug-cc-pVDZ yields similar excitation energies for the first vertically excited state at ADC(2) and CC2 level, with 6.23 eV and 6.37 eV, respectively. Increasing the basis from double to triple-zeta improves the excitation energies to 6.52 eV and 6.55 eV for ADC(2) and CC2, respectively. In general, the rotatory strengths are much more sensitive to augmentation of the basis set than the excitation energies. Even with aug-cc-pVDZ, the rotatory strength of the first transition is now within 20% of experiment, and within 15% for aug-cc-pVTZ, which has been overestimated by roughly 100% using non-augmented basis sets.

Moving to the doubly augmented, d-aug-cc-pVXZ series (X: D,T), the rotatory strength of the first excited state is within 10% of experiment for both ADC(2) and CC2 using d-aug-cc-pVDZ, but the excitation energy (< 0.04 eV) is hardly affected. Going to d-aug-cc-pVTZ, the rotatory strength is largely unaffected while the excitation energy is increased as was the case for the singly augmented aug-cc-pVTZ basis. However, double augmentation has substantial impact on the rotatory strengths of higher-lying excited states. For cc-pVXZ and aug-cc-pVXZ basis sets the second vertically excited state has an incorrect positive sign of the rotatory strength at ADC(2) and CC2 levels of theory, but is correctly described as negative using d-aug-cc-pVXZ basis sets. Higher-order methods like ADC(3), CCSD or CC3 reproduce the correct sign regardless of which basis set is employed. This illustrates the importance of diffuse functions as well as the degree of electron correlation included for a correct assignment of higher excited states.

Overall, the differences between the length and velocity forms of the rotatory strength are relatively small for the first electronic transition, i.e. on the order of $\sim 20 \leftrightarrow 10\%$ for cc-pVXZ, $\sim 10 \leftrightarrow 8\%$ for the aug-cc-pVXZ, and $\sim 10 \leftrightarrow 7\%$ for d-aug-cc-pVXZ at the ADC(2) and CC2 level of theory. The difference is on the same order of magnitude for energetically higher-lying excited states with minor exceptions (to see the effect on a shift in gauge-origin on the length gauge rotatory strength, see supporting information Fig. S5). The difference between the length and velocity forms of the oscillator strength is very similar to the one observed for the rotatory strengths.

(*R*)-methyloxirane. Comparison of the performance of the individual methods in the calculation of the ECD spectrum of methyloxirane when the d-aug-cc-pVDZ basis set is used reveals ADC(2) and CC2 to yield very similar spectra as obtained from the first 15 excitations calculated (Table S3 in the Supplementary Information). All spectra are shifted for the first state to correspond to

TABLE I. Transition energy, ω (eV), optical rotatory strength, R ($\times 10^{-40}$ c.g.s.) and oscillator strength f ($\times 10^{-3}$) of the lowest excited singlet states of methyloxirane and methylthiirane calculated at ADC and LR-CC levels using d-aug-cc-pVDZ.

Methyloxirane

	ADC(2)					ADC(2)-x					ADC(3)				
n	ω_{0n}	R^r_{0n}	R^∇_{0n}	f^r_{0n}	f^∇_{0n}	ω_{0n}	R^r_{0n}	R^∇_{0n}	f^r_{0n}	f^∇_{0n}	ω_{0n}	R^r_{0n}	R^∇_{0n}	f^r_{0n}	f^∇_{0n}
1	6.18	−13.5	−14.9	11.7	13.4	5.92	−15.1	−17.2	11.1	13.6	7.84	−13.3	−11.8	5.8	4.4
2	6.56	−0.8	−1.1	6.2	8.0	6.26	−2.8	−3.4	9.6	13.3	7.93	−12.8	−11.0	21.7	16.1
3	6.62	5.8	6.5	15.7	18.9	6.37	8.3	9.5	14.5	18.9	8.23	5.6	4.8	3.2	3.2
4	6.79	3.6	4.0	13.2	15.4	6.57	4.6	5.2	13.9	17.7	8.30	20.5	17.3	21.1	15.5
5	7.40	4.1	4.6	5.2	5.5	7.22	7.2	8.1	3.6	4.3	8.47	6.5	5.8	28.7	25.2
6	7.47	−1.8	−1.9	1.6	1.9	7.27	13.0	14.9	4.2	5.2	8.57	−15.5	−13.4	33.6	25.8
7	7.48	0.4	0.5	4.2	4.8	7.31	−4.4	−4.8	2.6	2.9	8.72	−3.4	−2.9	18.2	17.2
8	7.54	−0.3	−0.3	1.8	1.9	7.34	−1.7	−1.7	9.1	10.9	8.87	−8.6	−8.4	6.9	6.7
9	7.57	−0.8	−0.9	2.8	2.9	7.40	−0.5	−0.5	2.0	2.3	8.92	4.2	1.6	4.6	3.3

	CC2					CCSD					CC3[a]				
n	ω_{0n}	R^r_{0n}	R^∇_{0n}	f^r_{0n}	f^∇_{0n}	ω_{0n}	R^r_{0n}	R^∇_{0n}	f^r_{0n}	f^∇_{0n}	ω_{0n}	R^r_{0n}	R^∇_{0n}	f^r_{0n}	f^∇_{0n}
1	6.32	−15.9	−15.2	14.1	12.9	7.10	−15.0	−14.8	9.6	9.0	7.18	−19.4	−18.8	13.5	12.7
2	6.70	−1.3	−1.5	7.0	6.9	7.32	−6.4	−6.4	16.5	18.8	7.47	−3.8	−4.0	12.8	12.8
3	6.76	6.5	6.4	18.7	17.9	7.53	9.1	9.0	15.0	14.6	7.65	10.5	10.1	18.4	16.9
4	6.93	4.4	4.1	16.8	15.9	7.74	5.6	5.6	16.9	17.1	7.85	8.1	7.9	22.0	21.4
5	7.54	5.0	4.9	6.3	5.6	8.04	9.8	10.2	4.1	4.3					
6	7.61	−2.1	−1.9	1.9	1.8	8.38	0.8	0.9	2.2	2.1					
7	7.62	1.1	1.3	5.2	4.8	8.44	−6.4	−5.9	25.3	23.9					
8	7.66	8.5	9.3	2.7	2.9	8.47	−1.7	−2.2	16.1	14.9					
9	7.68	−0.9	−0.8	3.1	2.8	8.50	4.5	4.6	10.5	10.9					

Methylthiirane

	ADC(2)					ADC(2)-x					ADC(3)				
n	ω_{0n}	R^r_{0n}	R^∇_{0n}	f^r_{0n}	f^∇_{0n}	ω_{0n}	R^r_{0n}	R^∇_{0n}	f^r_{0n}	f^∇_{0n}	ω_{0n}	R^r_{0n}	R^∇_{0n}	f^r_{0n}	f^∇_{0n}
1	5.02	−1.8	−1.7	0.3	0.3	4.33	−1.4	−1.4	0.2	0.3	4.95	−1.2	−1.2	0.2	0.2
2	5.56	−4.7	−5.1	19.6	19.5	5.02	−6.3	−7.4	13.7	16.3	5.91	−5.2	−5.2	34.3	29.7
3	5.79	−5.3	−5.5	34.7	37.8	5.28	−5.3	−6.0	33.7	43.2	5.98	−6.9	−6.6	17.8	17.2
4	6.08	−0.3	−0.3	15.9	15.6	5.56	1.1	1.2	15.6	17.8	6.41	2.3	2.1	21.5	19.1
5	6.31	2.1	2.0	3.2	3.5	5.80	3.4	3.6	3.1	4.0	6.64	3.7	3.7	2.2	2.1
6	6.72	8.3	8.7	14.5	13.3	6.24	8.6	9.8	16.4	17.5	7.07	5.6	5.4	21.7	17.6
7	6.83	−0.1	−0.2	1.5	1.3	6.39	0.3	0.2	1.1	1.2	7.20	1.1	1.0	1.0	0.9
8	6.86	3.5	3.5	8.6	8.8	6.43	2.0	2.1	10.3	11.9	7.24	2.8	2.6	9.4	8.2
9	6.88	−1.2	−1.3	2.3	1.7	6.46	0.4	0.2	1.0	1.2	7.25	−1.9	−1.8	1.0	0.9

	CC2					CCSD					CC3[a]				
n	ω_{0n}	R^r_{0n}	R^∇_{0n}	f^r_{0n}	f^∇_{0n}	ω_{0n}	R^r_{0n}	R^∇_{0n}	f^r_{0n}	f^∇_{0n}	ω_{0n}	R^r_{0n}	R^∇_{0n}	f^r_{0n}	f^∇_{0n}
1	5.07	−2.2	−2.1	0.3	0.3	5.02	−1.2	−0.9	0.3	0.3	4.99	−1.5	−1.5	0.2	0.3
2	5.62	−5.7	−5.2	20.1	18.9	5.80	−5.6	−5.8	26.1	24.6	5.80	−8.5	−8.5	18.9	17.7
3	5.84	−5.4	−5.3	34.9	33.9	5.93	−6.1	−6.3	26.5	29.5					
4	6.14	0.0	0.0	17.2	15.3	6.31	0.6	0.5	19.0	18.3					
5	6.37	2.5	2.3	3.7	3.5	6.55	3.2	3.2	2.5	2.5					
6	6.77	8.3	8.6	15.2	14.5	6.96	6.9	7.2	19.9	17.5					
7	6.89	0.2	0.2	1.5	1.5	7.10	0.6	0.4	1.4	1.3					
8	6.92	4.0	3.9	9.1	8.6	7.13	5.1	4.9	5.3	4.9					
9	6.93	−1.2	−1.2	2.4	2.3	7.13	−2.3	−2.3	6.1	6.2					

[a] Calculated with aug-cc-pVDZ basis.

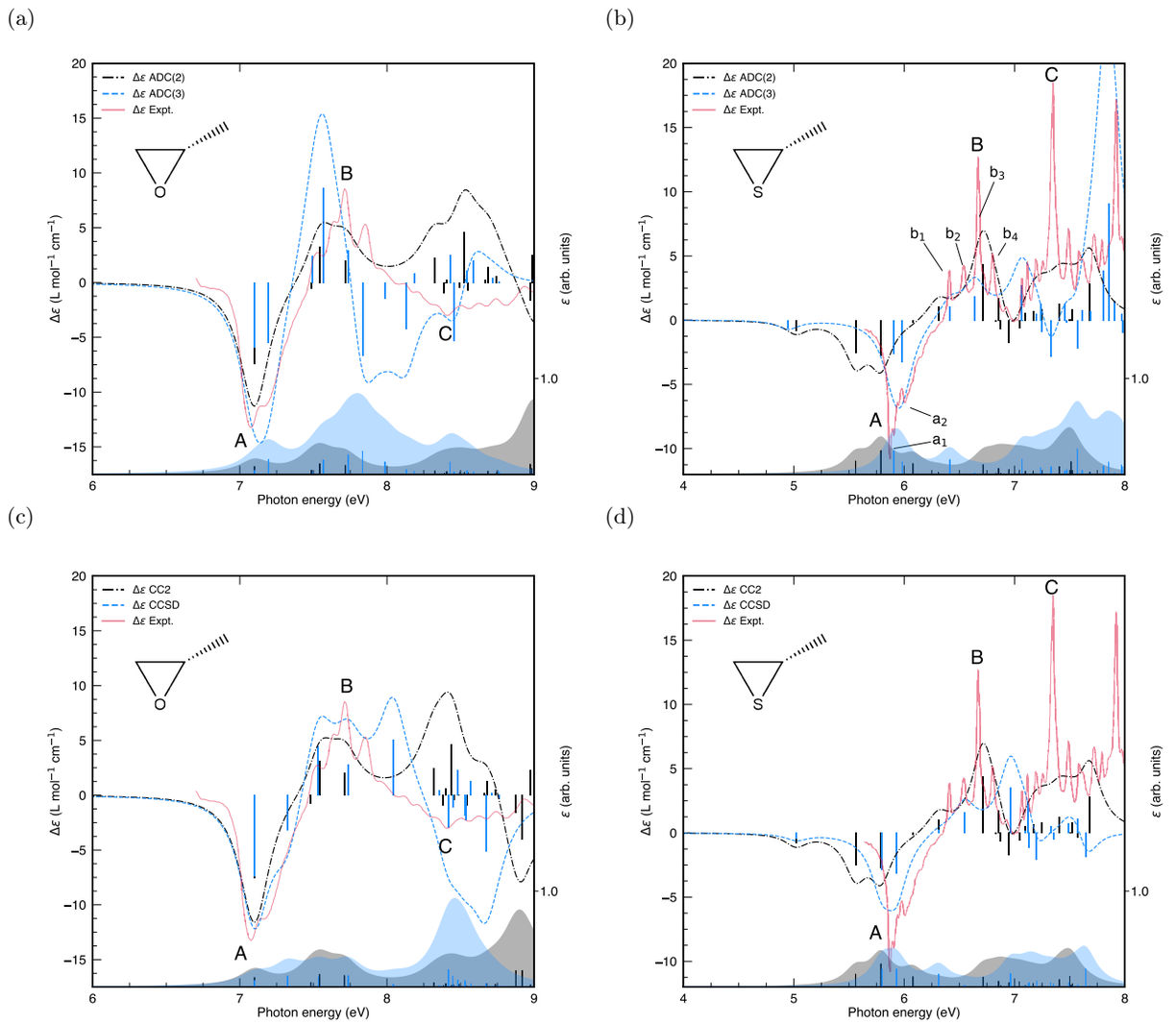

FIG. 2. ECD (top) and UV/VIS (bottom) spectra of methyloxirane (a and c) and methylthiirane (b and d) calculated with ADC(2), ADC(3), CC2, CCSD in the velocity gauge, using d-aug-cc-pVDZ. Methyloxirane spectra are shifted by +0.92 eV and −0.74 eV for ADC(2) and ADC(3), respectively, as well as +0.78 eV and −0.02 eV for CC2 and CCSD, respectively. The rotatory strength is scaled by a factor of 0.5. Experimental data (red line) are taken from Ref. 67.

the experimental value of 7.10 eV. The shifts required are +0.92 eV for ADC(2) and +0.78 eV for CC2, respectively. Two prominent features of the experimental spectrum, **A** and **B** are well reproduced by ADC(2) and CC2 (Fig. 2). Furthermore, at these levels of theory, **A-C** arise from oxygen lone-pair excitations to Rydberg orbitals. According to our calculations, **A** is a convolution of two states of negative amplitude, and **B** is a convolution of three states with an overall positive amplitude. Lastly, **C** corresponds to a convolution of three states and is incorrectly predicted as positive by both methods.

The spectra calculated at ADC(3) and CCSD level of theory are again shifted by −0.74 eV and −0.02 eV, respectively, for the first vertical excitation energy to match the experimental value. At these levels of theory, in addition to **A** and **B**, also **C** is correctly predicted as negative albeit red-shifted by ∼ 0.5 eV for ADC(3).

(*R*)-methylthiirane. Methylthiirane is the sulfur containing analog of methyloxirane, and again a high-quality experimental gas phase ECD spectrum is available,[67,68] as well as experimental vibrational circular dichroism (VCD)[78] and Raman optical activity (ROA)[79] spectra. The ECD spectrum and the optical rotatory dispersion have also been addressed in theoretical studies.[80,81] The experimental ECD spectrum of methylthiirane possesses three distinct features, **A**, **B**

and **C** in analogy to methyloxirane. Using the d-aug-cc-pVDZ basis set, ADC(2) and CC2 yield very similar transition energies and rotatory strengths for the energetically lowest 15 computed states (Table S4 in the Supplementary Information). All excited states correspond to electronic transitions from sulfur lone pair orbitals into Rydberg orbitals. ADC(2) and CC2 yield ECD spectra correctly predicting the signs of **A**, **B** and **C**. The excitation energies are red-shifted by roughly 0.4 eV in comparison to experiment (Fig. 2). The first peak arises from a weakly absorbing state with a negative rotatory strength, which has also been experimentally observed but was not shown in the experimental spectrum as it was barely visible. The first significant feature of the experimental spectrum, **A**, is a convolution of two peaks which are correctly predicted as negative but the amplitude is underestimated by a factor of two at these levels of theory. **B** and **C** correspond to convolutions of multiple states, the signs of which are correctly predicted using ADC(2) and CC2.

Proceeding to ADC(3), the excitation energies require no shift and transition amplitudes agree very well with experiment. The two electronic states constituting the spectral feature **A**, a_1 and a_2, lie within ∼0.02 eV of the experimental spectrum at the ADC(3) level, but, the rotatory strengths of these states appear to be swapped compared to experiment. Although, it cannot be excluded that these arise from vibrational effects. The improvement is of equal quality for CCSD, although slightly red-shifted compared to experiment. **B** consist of four vibronic peaks in the experimental spectrum. At ADC(3) level two excited electronic states are computed exhibiting the correct excitation energies and signs of their rotatory strengths. **C** is a convolution of several peaks in the experimental spectrum, and is incorrectly described as negative by both ADC(3) and CCSD.

B. ECD spectra of dimethyloxirane and dimethylthiirane

Also for dimethyloxirane and dimethylthiirane high-quality experimental gas phase ECD spectra are available[67,68] and show features similar to the ones of methyloxirane and methylthiirane. The excitation energies, oscillator and rotatory strengths calculated at the ADC(2), ADC(3), CC2 and CCSD levels of theory for the nine lowest excited states of (*R*,*R*)-dimethyloxirane and (*R*,*R*)-dimethylthiirane are collected in Table II (see Table S5-S8 in the supporting information for all excited states computed). The simulated ECD and UV/VIS spectra at the same levels of theory of the 15 energetically lowest excited states are shown in Fig. 3.

(*R*,*R*)-dimethyloxirane. At the ADC(2) and CC2 levels of theory using the d-aug-cc-pVDZ basis set, both methods produce very similar spectra for the energetically lowest 15 states computed, with the ADC(2) excitation energies red-shifted by $\sim 0.15 - 0.20$ eV compared to CC2. All spectra are shifted for the first state to correspond to the experimental value of 7.0 eV. The shifts required are +0.92 eV and +0.78 eV for ADC(2) and CC2, respectively. At these levels of theory, the vertical excited states arise exclusively from lone-pair orbital excitations from the oxygen atom into Rydberg orbitals. Further, the spectral feature **A** (Fig. 3) arises solely from the lowest transition, the excitation energy of which is red-shifted by ∼ 0.8 eV from experiment, reproduced as 6.08 eV and 6.22 eV for ADC(2) and CC2, respectively. The rotatory strength, however, is in reasonable agreement with experiment, although it is roughly overestimated by 40% for both ADC(2) and CC2. Furthermore, ADC(2) and CC2 show **B** arising solely from the second excited state for which the excitation energy is calculated at 6.38 eV and 6.53 eV for ADC(2) and CC2 respectively, which is again red-shifted by ∼ 0.9 eV compared to experiment. The rotatory strength is overestimated by an order of magnitude. The band **C**, at these levels of theory arises from the third and fourth excited states, which, in comparison with experiment are red-shifted by roughly 1 eV for both ADC(2) and CC2. **D** arises from the fifth and sixth excited states, which are again too low in energy by roughly 1.1 eV.

The spectra of the higher order methods ADC(3) and CCSD are also shifted to correspond to experiment. The shifts required are −0.81 eV and −0.07 eV for ADC(3) and CCSD, respectively. ADC(3) again yields higher excitation energies, as was already the case for methyloxirane. The CCSD excitation energies on the other hand agree to within ∼ 0.10 eV with experiment. At ADC(3) level, the spectral feature **A** arises from two states with negative rotatory strengths, separated by 0.10 eV. These peaks appear in agreement with the experimental ECD spectrum. We note that other studies have assigned these peaks to vibronic structures originating from up to two electronic states.[83] Furthermore, these two peaks are not reproduced in the CCSD spectrum which, alike ADC(2) and CC2, shows **A** arising from a single excited electronic state, whose width closely agrees with the experimental one. At ADC(3) level of theory, **B** is a convolution of the third and fourth excited state, the first sharply positive and latter negative. This results in a relatively weak positive feature, in reasonably good agreement with experiment. A similar convolution is observed at CCSD level, however of the second and third excited state. The larger energetic separation between the two states in CCSD results in a more intense positive **B**-band feature, whereas the negative component merges with the negative **C** band. **C** is again a convolution of many states at ADC(3) level resulting in broad positive band, not present in experiment, followed by blue-shifted negative peak. CCSD predicts the overall negative band of **C**, which is originating from the fourth and fifth excited states (with a shoulder due to the third one), in better agreement with experiment. **D** is correctly predicted as positive and arising from the tenth excited state using

TABLE II. Transition energy, ω (eV), optical rotatory strength, R ($\times 10^{-40}$ c.g.s.) and oscillator strength f ($\times 10^{-3}$) of the lowest excited singlet states of dimethyloxirane and dimethylthiirane calculated at ADC and LR-CC levels using d-aug-cc-pVDZ.

Dimethyloxirane

	ADC(2)					ADC(2)-x					ADC(3)				
n	ω_{0n}	R^r_{0n}	R^∇_{0n}	f^r_{0n}	f^∇_{0n}	ω_{0n}	R^r_{0n}	R^∇_{0n}	f^r_{0n}	f^∇_{0n}	ω_{0n}	R^r_{0n}	R^∇_{0n}	f^r_{0n}	f^∇_{0n}
1	6.08	−12.6	−14.0	8.0	10.4	5.87	−15.7	−18.3	8.5	12.2	7.85	−22.6	−20.9	13.1	11.0
2	6.38	14.6	16.3	10.6	13.3	6.18	17.7	20.9	11.6	16.0	7.95	−19.4	−19.7	8.1	8.4
3	6.57	−8.5	−9.3	8.6	10.7	6.45	−11.6	−13.1	11.5	15.6	8.16	22.1	17.3	10.2	6.2
4	6.65	−3.8	−4.1	1.2	1.5	6.50	−4.8	−5.4	1.5	1.9	8.23	−11.2	−9.5	9.1	5.6
5	7.16	4.6	5.0	14.7	15.9	6.98	−10.0	−10.1	2.3	2.3	8.33	1.1	1.0	18.3	16.1
6	7.22	0.3	0.5	0.0	0.0	7.22	0.3	0.5	0.0	0.0	8.39	1.6	2.3	0.2	0.5
7	7.26	−8.2	−8.6	9.1	9.8	7.26	−8.2	−8.6	9.1	9.8	8.46	−21.8	−18.9	26.6	19.9
8	7.27	1.8	1.9	2.4	3.0	7.27	1.7	1.9	2.4	3.0	8.48	23.0	22.3	22.7	21.1
9	7.29	2.6	2.8	0.8	0.9	7.29	2.6	2.8	0.8	0.9	8.79	−8.8	−10.0	1.4	1.8

	CC2					CCSD				
n	ω_{0n}	R^r_{0n}	R^∇_{0n}	f^r_{0n}	f^∇_{0n}	ω_{0n}	R^r_{0n}	R^∇_{0n}	f^r_{0n}	f^∇_{0n}
1	6.22	−15.0	−14.2	10.8	10.1	7.07	−16.3	−16.3	9.8	10.3
2	6.53	16.5	16.0	12.3	11.6	7.35	16.2	15.9	12.2	11.7
3	6.71	−9.8	−9.8	10.0	10.0	7.46	−10.1	−11.0	12.6	14.2
4	6.79	−4.1	−4.4	1.3	1.5	7.66	−4.8	−4.8	1.0	0.9
5	7.30	5.9	5.8	18.7	17.1	7.76	3.5	3.0	9.1	8.5
6	7.34	−12.4	−11.1	3.7	3.0	8.12	3.5	3.0	9.1	8.5
7	7.37	0.8	1.2	0.1	0.2	8.20	−16.4	−16.0	6.0	5.7
8	7.40	2.2	2.2	3.2	3.3	8.23	10.6	10.7	22.8	22.8
9	7.40	−3.6	−3.4	8.6	7.6	8.31	0.2	0.2	1.2	1.1

Dimethylthiirane

	ADC(2)					ADC(2)-x					ADC(3)				
n	ω_{0n}	R^r_{0n}	R^∇_{0n}	f^r_{0n}	f^∇_{0n}	ω_{0n}	R^r_{0n}	R^∇_{0n}	f^r_{0n}	f^∇_{0n}	ω_{0n}	R^r_{0n}	R^∇_{0n}	f^r_{0n}	f^∇_{0n}
1	5.03	5.0	5.7	0.2	0.2	4.33	3.5	4.4	0.1	0.1	4.97	0.7	0.1	0.0	0.0
2	5.62	−10.0	−11.0	21.3	21.5	5.06	−11.7	−13.9	15.2	18.3	5.99	−6.9	−7.4	41.0	36.2
3	5.94	−20.5	−20.7	32.1	33.5	5.40	−18.0	−19.8	31.8	39.7	6.13	−20.6	−19.0	12.1	11.2
4	6.00	1.0	1.0	25.0	24.1	5.45	3.2	3.3	21.2	23.9	6.37	5.3	4.9	26.2	21.8
5	6.30	−5.8	−6.4	2.7	3.2	5.77	−5.3	−6.4	2.4	3.5	6.66	−2.5	−1.8	0.7	0.4
6	6.53	10.3	11.0	3.1	2.9						6.89	6.1	6.1	8.6	6.6
7	6.68	5.5	5.4	8.4	8.3						7.06	11.3	10.7	9.8	8.9
8	6.72	3.8	3.8	8.4	8.4						7.13	2.9	2.7	10.7	9.1
9	6.73	−1.1	−0.6	0.2	0.1						7.14	−2.9	−3.2	1.2	1.4

	CC2					CCSD				
n	ω_{0n}	R^r_{0n}	R^∇_{0n}	f^r_{0n}	f^∇_{0n}	ω_{0n}	R^r_{0n}	R^∇_{0n}	f^r_{0n}	f^∇_{0n}
1	5.08	4.4	4.5	0.1	0.1	5.04	2.4	3.1	0.0	0.1
2	5.63	−8.0	−7.2	24.3	23.2	5.82	−5.2	−5.3	35.6	34.9
3	5.88	−19.6	−19.0	25.6	24.5	6.01	−21.0	−21.7	13.5	15.4
4	6.00	−0.2	−0.2	22.7	20.4	6.18	1.7	1.6	22.5	21.7
5	6.26	−5.5	−5.6	2.3	2.4	6.46	−3.4	−3.4	1.0	0.9
6	6.59	10.6	10.6	3.6	3.6	6.79	8.6	9.0	6.6	5.2
7	6.74	6.6	6.4	9.6	9.0	6.96	9.5	9.1	11.2	10.4
8	6.79	4.3	4.2	9.1	8.8	7.01	3.2	3.2	9.9	9.3
9	6.79	−1.4	−1.1	0.3	0.2	7.02	−2.3	−2.3	0.7	0.7

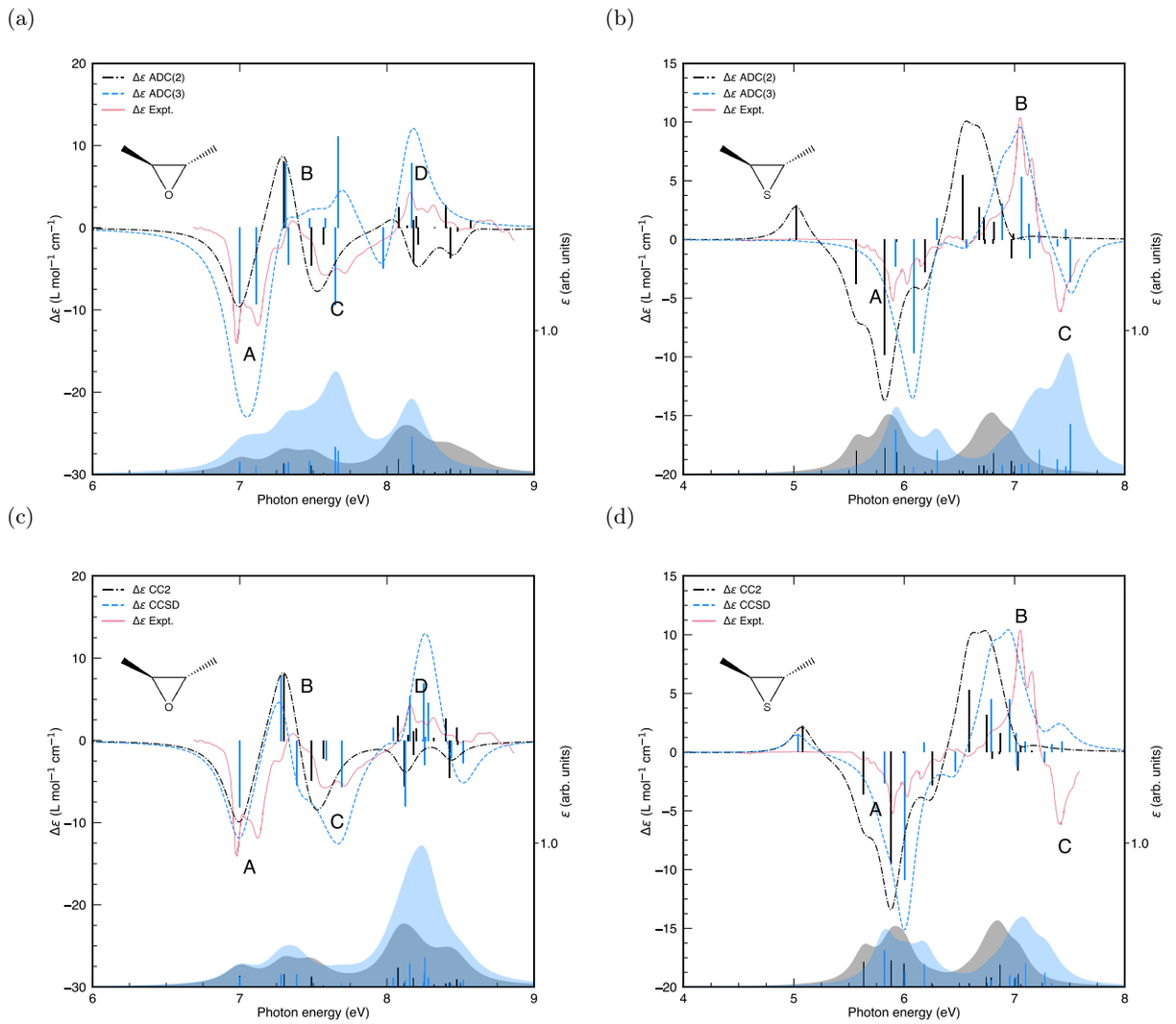

FIG. 3. ECD (top) and UV/VIS (bottom) spectra in of dimethyloxirane (a and c) and dimethylthiirane (b and d) calculated with ADC(2), ADC(3), CC2, CCSD in the velocity gauge using the d-aug-cc-pVDZ basis set. Dimethyloxirane spectra are shifted by +0.92 eV and −0.81 eV for ADC(2) and ADC(3), respectively, as well as +0.78 eV and −0.07 eV for CC2 and CCSD, respectively. The rotatory strength is scaled by a factor of 0.5. Experimental data (red line) for dimethyloxirane are taken from Ref. 67 and for dimethylthiirane from Ref. 82.

ADC(3) and a convolution of many states using CCSD.

(*R*,*R*)-dimethylthiirane. The three bands, **A-C**, of dimethylthiirane are again investigated using the d-aug-cc-pVDZ basis set and are characterised by lone-pair excitations into Rydberg orbitals by ADC(2) and CC2. The excitation energy of the first excited state is calculated as 5.03 eV and 5.08 eV, by ADC(2) and CC2, respectively, which are blue-shifted by roughly 0.5 eV, compared to the reported experimental value of 4.5 eV. The first rotatory strength exhibits an error of more than an order of magnitude, 5.7 ($\times 10^{-40}$ c.g.s.) and 4.3 ($\times 10^{-40}$ c.g.s.) for ADC(2) and CC2, respectively, compared to the experimental value of 0.1 ($\times 10^{-40}$ c.g.s.).[82] However, this is a weakly active state and as such experimental limitations may also play a role.

The first distinct feature **A** in the experimental spectrum is a convolution of the second to fifth excited states at these levels of theory. The second feature, **B**, is a convolution of the sixth to eighth excited state, and the third band, **C**, arises from higher-lying excited states above the eighth state. It is interesting to recognize that the calculated spectra at ADC(2) and CC2 levels could be mistaken as that of a red-shifted (S,S)-dimethylthiirane, however, this is not the case for the higher order methods.

Using ADC(3) and CCSD with the d-aug-cc-pVDZ basis set the lowest excitation energy remains mostly unaltered at 4.97 eV and 5.04 eV, respectively. Unlike ADC(2), ADC(3) yields a rotatory strength for the first weak peak of similar magnitude to that of the experiment, deviating by ∼10%, however, still overestimated by an order of magnitude for CCSD. Here, 14 excited states are computed and for the first and second band feature **A** and **B**, ADC(3) results agree well with experiment, although the rotatory strength of **A** is still overestimated by a factor of two. Significantly, the last band feature, **C**, is correctly predicted as negative at ADC(3) level resulting from a convolution of several excited states but incorrectly predicted as positive using CCSD. We note however that more excited states may be needed at the CCSD level to reproduce this spectral region.

C. ECD spectra of H_2O_2 and H_2S_2

The chiro-optical properties of H_2O_2 and H_2S_2 have been the subject of benchmark calculations due to their small size and complex electronic structure.[14,84,85] The dependence of the optical rotatory strength on the dihedral angle of H_2S_2 has been studied at the CIS level. It was discovered that H_2S_2 has degenerate excited states at a dihedral angle of $\sim 90°$ which are poorly described using a HF wavefunction. Later the performance of various density functionals was benchmarked against MRCI and CC2 calculations.[86] As can be expected from a sulfur containing chromophore, low-lying excitations are characterized by Rydberg to a certain extent.[86] Fewer studies have been carried out on H_2O_2 and for neither molecule the ECD spectra have been simulated using a third order *ab initio* method. The excitation energies, oscillator and rotatory strengths calculated at the ADC(2), ADC(3), CC2, CCSD and CC3 levels of theory for the nine lowest excited states of H_2O_2 and H_2S_2 are collected in Table III (see Table S9-S12 in the supporting information for all excited states computed). The simulated ECD and UV/VIS spectra at the same levels of theory of the 15 energetically lowest excited states are shown in Fig. 4.

H_2O_2. For H_2O_2, the optimized geometrical parameters at MP2/d-aug-cc-pVTZ level are r(OO): 1.452 Å, r(OH): 0.967 Å, ϕ(OOH): 99.67° and Φ(HOOH): 112.16°. Due to the lack of experimental data, CC3 and ADC(3) serve as references when analysing the performance of ADC(2) and CC2 in the simulation of the ECD spectra. Five distinct features, **A**-**E**, are analyzed which all correspond to lone-pair excitations into Rydberg orbitals.

ADC(2) and CC2 yield very similar ECD spectra for the energetically lowest 15 singlet states. The first feature, **A**, at the ADC(2) and CC2 levels of theory, arises from the first electronic excited state and the excitation energy and rotatory strengths are calculated to within 0.03 eV and ∼ 15% from the corresponding CC3 excitation energy and rotatory strength, respectively. The second spectral feature, **B**, arises from the second excited state and likewise agrees well between ADC(2) and CC2, but is red-shifted for both methods by ∼ 0.5 eV and the rotatory strengths are within ∼ 10%, with respect to CC3 energies and rotatory strengths. **C** corresponds to the third excited state and ADC(2) and CC2 energies are blue-shifted by ∼0.04 eV and rotatory strengths are within ∼10% to those at CC3 level, however due to the larger energetic gap between the third and fourth excited state at the CC3 level, the convoluted spectra at ADC(2) and CC2 levels show **C** overestimated by a factor of 2. **D** corresponds to the fourth excited state and is red-shifted by roughly 0.4 eV at ADC(2) and CC2 levels, with rotational strengths calculated to within ∼10%, compared with CC3 energies and rotatory strengths. Lastly **E** is caused by the fifth excitation and is red-shifted by ∼ 0.5 eV with rotatory strengths underestimated by ∼50% and ∼30% for ADC(2) and CC2, respectively, as compared with CC3. It is noteworthy that **E** could be mistaken as positive, at the ADC(2) and CC2 levels, caused by the sixth excitation.

For the higher order methods ADC(3), CCSD and CC3 the first excited state responsible for the spectral feature **A** has an excitation energy of 5.95 eV, 6.14 eV and 6.08 eV, respectively. For the second band, **B**, ADC(3) and CCSD are blue-shifted by 0.5 eV, compared to ADC(2) and CC2, however, at ADC(3) level the sign of the transition is positive. This reversal can be explained by the dependence of the rotatory strength on the H_2O_2 structural parameters, specifically the length of the oxygen-oxygen bond. Contraction of this bond by 1.8 pm from its MP2 equilibrium geometry (1.452 Å) interchanges the second and third excitations, i.e. **B** and **C**, at ADC(3) level, which then fall directly into reasonable agreement with the CCSD and CC3 results (Fig. 4). An identical contraction leaves CCSD and CC3 excited states invariant, showing a unique dependence on the structural parameters for ADC(3). **D** and **E** correspond to the same excited states as those calculated using ADC(2) and CC2, and agree well between ADC(3) and CC3, after contraction of the oxygen-oxygen bond.

H_2S_2. The optimized geometrical parameters for H_2S_2 at MP2/d-aug-cc-pVTZ are r(SS): 2.067 Å, r(SH): 1.340 Å, ϕ(SSH): 97.77° and Φ(HSSH): 90.89°. Here, the ADC(2) and CC2 results are again very similar. Four band features are evident in the broadened ECD spectra of the 15 energetically lowest excited states computed, all of which consist of near degenerate n-Rydberg excited states of alternating sign. **A** corresponds to the first and second excited state, **B** the third and fourth, **C** the fifth and sixth, all separated by ∼ 0.02 eV and **D** is a convolution of multiple narrowly separated higher-lying states.

At ADC(3) and CCSD levels, **A**-**D** remain mostly unaltered, with ADC(3) shifting **A**, **B**, **C** and **D** by −0.25 eV, −0.10 eV, −0.05 eV and +0.01 eV, respectively. A smaller shift of opposite trend is observed for CCSD with **A**, **B**, **C** and **D** being shifted by +0.02 eV, −0.04 eV, −0.08 eV and −0.15 eV, respectively. Of the four states

TABLE III. Transition energy, ω (eV), optical rotatory strength, R ($\times 10^{-40}$ c.g.s.) and oscillator strength ($\times 10^3$) of the lowest singlet excited states of H_2O_2 and H_2S_2 calculated at ADC and LR-CC levels using the d-aug-cc-pVTZ basis set.

H_2O_2

	ADC(2)					ADC(2)-x					ADC(3)				
n	ω_{0n}	R^r_{0n}	R^∇_{0n}	f^r_{0n}	f^∇_{0n}	ω_{0n}	R^r_{0n}	R^∇_{0n}	f^r_{0n}	f^∇_{0n}	ω_{0n}	R^r_{0n}	R^∇_{0n}	f^r_{0n}	f^∇_{0n}
1	6.08	−10.8	−9.8	6.1	7.3	5.20	−8.5	−9.8	3.7	5.0	5.95	−6.8	−6.0	2.9	2.3
2	6.57	−18.7	−16.1	4.4	5.4	6.04	−16.6	−20.8	4.8	6.6	7.07	9.1	7.8	11.8	8.3
3	7.25	16.5	16.0	13.5	11.3	6.27	14.6	15.4	7.2	6.3	7.35	−14.7	−14.6	3.2	3.3
4	7.58	33.2	30.9	10.9	12.6	7.06	32.3	37.5	9.4	12.7	8.25	31.9	29.5	14.6	12.5
5	7.91	−9.4	−10.0	2.9	2.6	7.35	−11.0	−11.2	5.7	5.9	8.72	−17.4	−16.0	4.8	4.0
6	8.33	−0.1	−0.1	14.7	16.0	7.99	−0.2	−0.2	15.5	18.0	9.66	13.7	12.6	21.6	18.8
7	8.54	0.3	0.3	6.5	6.8	8.18	1.9	2.1	8.0	9.3	10.06	1.0	−0.1	136.0	127.1
8	8.79	0.1	0.0	5.6	5.7	8.32	8.7	8.8	18.0	18.9	10.06	0.1	0.1	0.2	0.1
9	8.86	6.9	6.3	15.3	14.2	8.55	−1.3	−2.0	1.0	1.0	10.30	2.3	2.1	12.6	10.6

	CC2					CCSD					CC3[a]				
n	ω_{0n}	R^r_{0n}	R^∇_{0n}	f^r_{0n}	f^∇_{0n}	ω_{0n}	R^r_{0n}	R^∇_{0n}	f^r_{0n}	f^∇_{0n}	ω_{0n}	R^r_{0n}	R^∇_{0n}	f^r_{0n}	f^∇_{0n}
1	6.08	−11.3	−11.1	6.5	6.4	6.14	−9.2	−11.3	4.2	6.4	6.08	−9.4	−9.8	4.0	4.3
2	6.60	−18.6	−18.4	5.4	5.0	7.10	−19.9	−21.3	7.5	8.1	7.09	−19.8	−19.8	8.6	8.5
3	7.25	17.1	17.1	13.3	11.2	7.30	16.1	18.7	8.2	8.1	7.21	16.2	16.8	6.5	6.6
4	7.61	34.5	33.5	13.4	12.6	8.06	33.3	33.3	14.1	14.1	8.06	34.3	33.6	14.2	13.6
5	7.93	−10.7	−9.7	3.3	2.7	8.49	−14.2	−13.3	3.8	3.4	8.46	−15.0	−14.7	4.4	4.3
6	8.36	0.3	0.4	17.7	16.0	9.06	−0.6	−0.6	20.7	21.1					
7	8.57	0.7	0.7	7.3	7.1	9.27	−0.3	−0.3	10.1	9.6					
8	8.82	0.1	−0.2	5.9	5.3	9.40	12.5	12.3	24.6	23.9					
9	8.89	7.4	6.8	16.9	13.7	9.64	1.1	0.6	2.3	2.1					

H_2S_2

	ADC(2)					ADC(2)-x					ADC(3)				
n	ω_{0n}	R^r_{0n}	R^∇_{0n}	f^r_{0n}	f^∇_{0n}	ω_{0n}	R^r_{0n}	R^∇_{0n}	f^r_{0n}	f^∇_{0n}	ω_{0n}	R^r_{0n}	R^∇_{0n}	f^r_{0n}	f^∇_{0n}
1	5.01	−5.5	−6.3	4.4	5.9	4.18	−4.0	−5.3	3.4	6.1	4.77	−5.0	−5.3	3.3	3.8
2	5.03	14.5	14.2	13.4	12.4	4.21	11.7	13.0	10.2	12.5	4.79	13.9	12.6	10.6	8.5
3	6.08	64.1	68.3	13.6	15.4	5.41	58.4	69.0	9.8	13.6	5.99	57.1	59.3	12.6	13.6
4	6.10	−72.8	−76.7	18.1	19.7	5.43	−66.2	−77.5	13.3	17.9	6.00	−64.2	−66.1	15.2	16.0
5	6.94	−27.7	−30.5	3.8	4.7	6.19	−25.9	−31.5	3.5	5.2	6.88	−21.7	−24.4	1.8	2.3
6	6.92	31.4	34.5	15.2	16.2	6.2	31.7	38.6	10.5	14.2	6.87	17.0	19.4	8.8	8.4
7	7.78	−19.0	−18.5	124.0	117.8	7.2	4.5	4.3	200.7	205.9	7.79	10.3	9.9	14.0	13.0
8	7.78	11.1	10.5	6.8	6.1	7.2	12.8	12.7	5.4	5.4	7.80	−16.3	−15.6	223.4	203.6
9	7.82	−16.9	−15.9	4.7	4.2	7.3	−18.2	−18.4	7.9	8.1	7.84	8.0	7.2	51.1	45.9

	CC2					CCSD					CC3[a]				
n	ω_{0n}	R^r_{0n}	R^∇_{0n}	f^r_{0n}	f^∇_{0n}	ω_{0n}	R^r_{0n}	R^∇_{0n}	f^r_{0n}	f^∇_{0n}	ω_{0n}	R^r_{0n}	R^∇_{0n}	f^r_{0n}	f^∇_{0n}
1	4.98	−5.8	−5.6	4.6	4.3	4.96	−6.3	−7.4	3.9	5.5	4.86	−6.0	−5.4	3.9	3.2
2	5.00	13.7	12.4	13.1	10.3	4.98	14.0	14.2	11.2	10.8	4.89	13.1	12.4	10.8	9.7
3	6.05	63.5	64.8	13.7	14.2	6.09	60.3	62.8	13.7	14.8	6.01	59.3	58.6	12.6	12.3
4	6.06	−72.3	−72.8	18.2	18.1	6.10	−68.0	−70.3	16.7	17.7	6.02	−67.3	−66.8	15.9	15.7
5	6.90	−28.8	−28.2	4.1	4.0	6.98	−23.5	−26.5	2.3	2.9					
6	6.88	31.7	29.9	15.4	14.6	6.96	20.1	22.4	11.1	11.2					
7	7.63	−8.7	−8.5	78.8	74.3	7.78	−6.4	−6.4	93.7	92.9					
8	7.65	7.7	7.1	1.7	1.5	7.79	8.9	8.7	2.7	2.6					
9	7.70	−12.5	−11.8	39.1	35.4	7.82	−15.1	−14.7	60.1	57.2					

[a] Calculated with aug-cc-pVDZ basis.

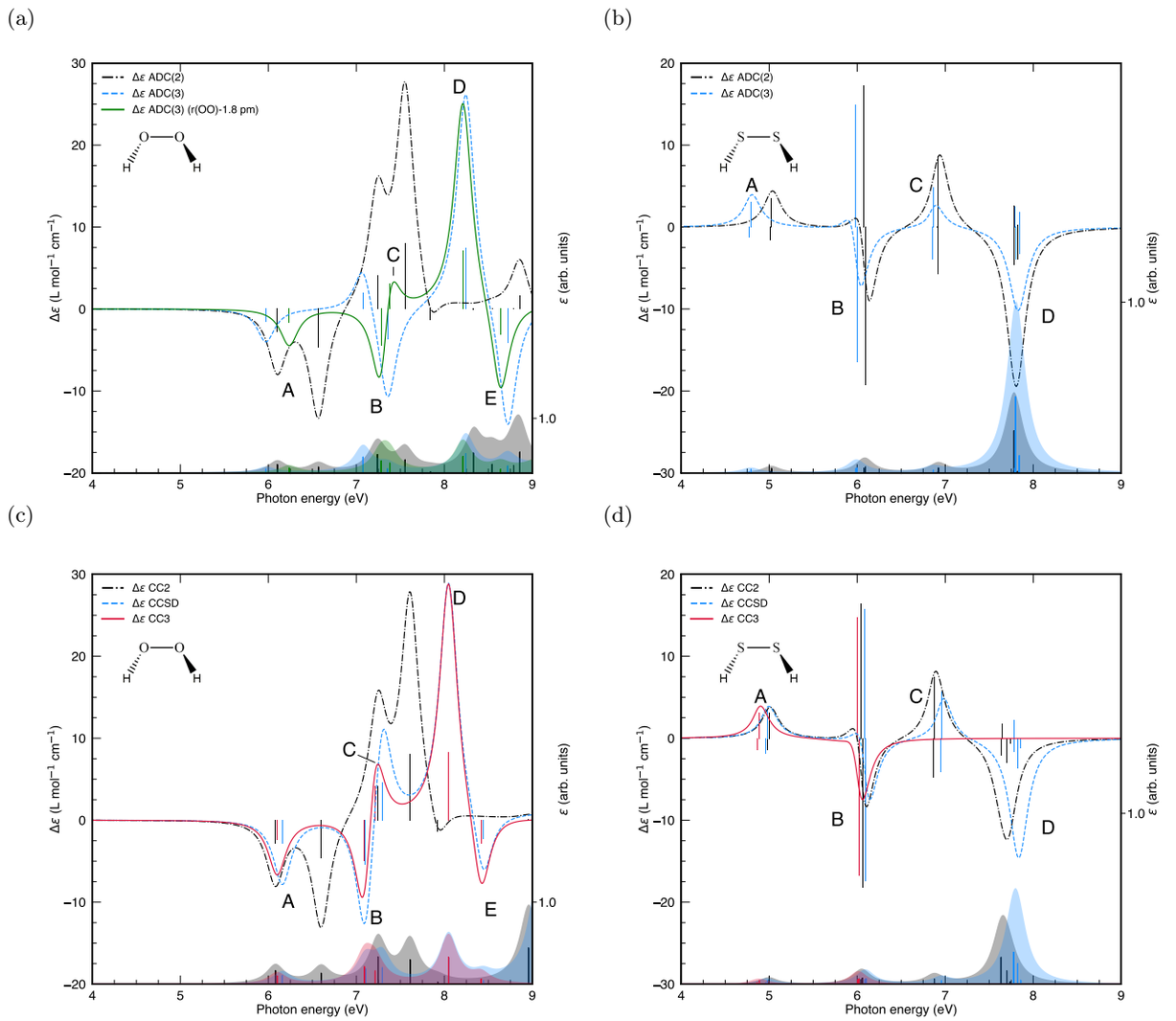

FIG. 4. ECD (top) and UV/VIS (bottom) spectra of H_2O_2 (a and c) and H_2S_2 (b and d) calculated with ADC(2), ADC(3), CC2, CCSD and CC3 in the velocity gauge using the aug-cc-pVTZ basis set for CC3 and d-aug-cc-pVTZ for all others. The oxygen-oxygen bond has been contracted by 1.8 pm in (a) (green line). The rotatory and oscillator strength is scaled by a factor of 0.25 and 0.5 respectively.

converged at CC3 level the excitation energy of **A** is blue-shifted compared to ADC(3) and red-shifted compared with CCSD, both by 0.1 eV. The rotatory strength of **A** is of equal quality for both ADC(3) and CCSD level with ADC(3) in slightly closer agreement. The CC3 energies of **B** are blue-shifted by 0.02 eV from ADC(3) and red-shifted 0.09 eV from CCSD with similar rotatory strength. Using the ADC(3) and CCSD spectra as references, ADC(2) and CC2 are shown to do adequate jobs in reproducing **A**-**D**.

D. ECD spectrum of solvated Epinephrine

Only the D-enantiomer of epinephrine (commonly known as adrenaline) is biologically relevant yet organic synthesis produces a racemic mixture of both enantiomers.[87] An efficient method to obtain enantiopure D-epinephrine is via HPLC separation in combination with ECD spectroscopy.[34] To demonstrate the general ability of our implementation of rotatory strengths within ADC to simulate the ECD spectra of solvated molecules, the solution spectrum of L-epinephrine in water is computed using a conductor-like polarizable continuum model (PCM) for water.[88,89] It is clear that for a

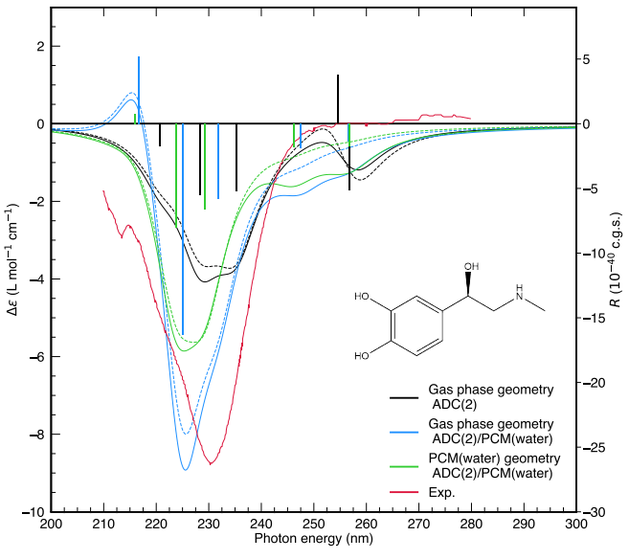

FIG. 5. ECD spectra of (L)-epinephrine calculated with ADC(2) with and without PCM in the length (solid line) and velocity (dashed line) gauges using the aug-cc-pVDZ basis set. Rotatory strengths are in the length gauge. The reference experimental data (red line) is the water solution spectrum taken from Ref. 34.

more thorough investigation, explicit water epinephrine interactions need to be considered, however, for a qualitative agreement and a proof-of-concept, the PCM approach suffices. The geometry of the L-epinephrine enantiomer was optimized using CAM-B3LYP/cc-pVTZ with and without PCM (the converged geometry in both cases corresponds to the AG1a conformer using the nomenclature adopted in Ref 90). The ECD spectra of these molecular systems were then computed at the ADC(2)/aug-cc-pVDZ/PCM(water) and ADC(2)/aug-cc-pVDZ levels of theory for the five energetically lowest excited states as shown in Fig. 5 (see Table S13 for numerical values). All states essentially correspond to $\pi\pi^*$ excitations with contributions from the oxygen/nitrogen lone pair into π^*-orbitals of the phenyl ring.

Two bands are seen in the experimental spectrum, one weakly positive peak centered around 270 nm and one broad negative peak centered around 230 nm. The band at 270 nm is however not unambiguously assignable in the experiment and may well correspond to noise. Using the gas-phase geometry at ADC(2)/aug-cc-pVDZ level, the second band of the ECD spectrum is clearly reproduced as a convolution of the third to fifth vertically excited states. The first band is a convolution of the first two excited states producing an overall negative band.

Including the PCM for water solvation for the calculation of the spectrum only, leads to a blue-shift of the center of the second band and drastically alters the computed rotatory strengths, which falls inline with the experimental spectrum, however, with the first band again predicted as a weakly absorbing negative band. Using the PCM for both geometry optimization as well as the calculation of the ECD spectrum yields a very similar spectrum to that obtained using the gas-phase geometry, showing that the optimized geometry is only negligibly influenced by solvation.

The difference between the length and velocity gauges for the energetically lowest excited states are as large as a factor of two but small in absolute terms, owing to the weak absorption, which can already originate from the incompleteness of the one-particle basis set. For energetically higher states with higher absorption, the gauges agree acceptably well, with deviations of ∼15%. For all states, the sign of the rotatory strength remains consistent.

E. ECD spectra of camphor, norcamphor and fenchone

Camphor and the structurally related molecules, norcamphor and fenchone have long been used as molecular standards for ECD calibrations[91–95] and their characteristic ECD spectra as well as VCD spectra have been extensively explored.[28,96–99]To the best of our knowledge, the ECD spectra of these molecules have not been calculated using high-level *ab initio* methods. The excitation energies, oscillator and rotatory strengths calculated at the ADC(2) and ADC(3) levels of theory for the nine lowest excited states of camphor, norcamphor and fenchone are collected in Table IV. The simulated ECD and UV/VIS spectra at the same levels of theory of the 10 energetically lowest excited states of the same molecules are shown in Fig. 6.

(1*R*)-camphor. As seen in Fig. 6, the ECD spectrum of (1R)-camphor in gas phase is fully reproduced using ADC(3)/aug-cc-pVDZ with the ten lowest lying excited states computed. The signs of the three bands (**A**-**C**), are all correctly predicted and the simulated ECD spectral amplitudes are in good agreement with experiment. We shift the simulated ECD spectrum -0.32 eV to correspond with experiment. The first peak **A** is caused by the energetically lowest excited state. Although it is a dark state in the UV/VIS spectrum, it becomes visible in the ECD spectrum due to its large magnetic transition dipole moment. The rotatory strength of this band matches well with that of experiment. The second band **B** appears as a vibrationally resolved peak in the experimental spectrum and is calculated as a convolution of the second to fifth excited electronic state which match closely in amplitude. **C** arises from the sixth to ninth excitation. All excited states correspond to n-Rydberg excitations.

At the ADC(2)/aug-cc-pVDZ level, **A**, **B** and **C** arise from the same states as those computed at ADC(3) level with identical signs. We shift the spectrum -0.08 eV to correspond with experiment. The rotatory strength of **A**, at this level of theory, matches well with experiment and roughly overestimates ADC(3) by a factor of 2. **B** and **C** are both red-shifted with respect to experiment

TABLE IV. Transition energy, ω (eV), optical rotatory strength, R (10^{-40} c.g.s.) and oscillator strengths ($\times 10^{-3}$) of the ten lowest electronic transitions of camphor, norcamphor and fenchone calculated at ADC(3) and ADC(2) levels of theory using the aug-cc-pVDZ basis set for camphor and fenchone and the d-aug-cc-pVDZ basis set for norcamphor.

ADC(3)

	(1*R*)-camphor					**(1*R*)-norcamphor**					**(1*R*)-fenchone**				
n	ω_{0n}	R^r_{0n}	R^∇_{0n}	f^r_{0n}	f^∇_{0n}	ω_{0n}	R^r_{0n}	R^∇_{0n}	f^r_{0n}	f^∇_{0n}	ω_{0n}	R^r_{0n}	R^∇_{0n}	f^r_{0n}	f^∇_{0n}
1	4.42	3.2	1.8	0.1	0.1	4.33	0.3	−0.5	0.2	0.1	4.38	−2.4	−3.0	0.0	0.0
2	6.67	4.7	3.6	12.3	9.7	6.65	−3.3	−2.8	14.3	11.3	6.58	−0.4	−0.2	1.5	2.0
3	7.11	−1.4	−1.3	16.6	15.4	7.23	15.0	13.6	12.5	9.8	6.99	10.2	9.2	27.9	21.7
4	7.14	3.4	3.0	7.1	6.0	7.27	3.7	3.9	15.5	15.1	7.05	−4.5	−4.3	21.0	17.6
5	7.21	1.3	1.2	23.5	18.8	7.33	−2.1	−2.0	7.9	6.4	7.11	5.9	5.2	5.2	4.0
6	7.66	−4.3	−4.1	9.0	8.4	7.86	−1.0	−1.2	12.9	10.3	7.57	1.5	1.4	9.5	8.4
7	7.80	1.4	1.3	9.4	7.7	7.91	−5.9	−5.1	29.0	24.7	7.68	0.6	0.5	1.8	1.5
8	7.81	−0.1	1.1	26.1	19.8	7.98	0.0	−0.3	3.8	3.9	7.69	−5.9	−5.6	4.7	4.2
9	7.85	−5.4	−4.6	14.8	10.7	8.07	−4.2	−3.0	2.2	1.2	7.75	1.4	1.4	22.0	18.8
10	7.89	7.6	6.2	7.5	4.9	8.13	−4.7	−3.5	18.6	12.9	7.79	0.4	0.4	31.7	27.8

ADC(2)

	(1*R*)-camphor					**(1*R*)-norcamphor**					**(1*R*)-fenchone**				
n	ω_{0n}	R^r_{0n}	R^∇_{0n}	f^r_{0n}	f^∇_{0n}	ω_{0n}	R^r_{0n}	R^∇_{0n}	f^r_{0n}	f^∇_{0n}	ω_{0n}	R^r_{0n}	R^∇_{0n}	f^r_{0n}	f^∇_{0n}
1	4.18	5.2	5.2	0.2	0.2	4.09	0.6	0.3	0.2	0.1	4.16	−2.1	−2.5	0.0	0.0
2	5.54	2.0	2.3	9.6	11.8	5.47	−1.6	−1.8	9.4	11.9	5.44	0.4	0.3	2.2	1.9
3	5.92	−0.4	−0.4	6.5	6.5	5.97	10.0	10.8	12.3	14.0	5.79	2.9	3.3	14.6	15.7
4	5.97	1.0	0.9	5.4	5.9	5.99	−0.3	−0.2	2.9	2.9	5.84	−0.4	−0.4	12.7	13.8
5	6.01	1.5	1.4	15.4	17.3	6.03	−1.6	−1.8	3.1	3.4	5.92	3.0	3.2	2.1	2.3
6	6.52	−0.7	−0.7	0.9	1.2	6.46	0.2	0.4	4.8	5.6	6.37	0.9	0.9	7.2	6.8
7	6.59	3.1	3.3	3.2	3.7	6.51	2.0	2.2	2.0	2.5	6.47	−0.2	−0.4	1.8	1.9
8	6.63	−0.9	−1.0	4.2	4.6	6.53	−0.2	−0.5	0.7	0.9	6.48	−1.6	−1.6	0.6	0.6
9	6.65	−2.6	−2.8	2.6	3.2	6.57	0.0	−0.1	0.1	0.1	6.54	0.0	−0.1	8.8	9.4
10	6.74	0.6	0.9	13.4	15.5	6.60	0.2	0.2	0.2	0.2	6.58	−1.4	−1.4	25.2	26.7

by $\sim$ 0.8 eV and $\sim$ 1 eV, respectively. The rotatory strength of **B** and **C** is calculated to roughly half and roughly one quarter, respectively, as those at ADC(3) level.

(1*R*)-norcamphor. Results of equal quality are found for (1*R*)-norcamphor, except, here, excitation energies are blue-shifted by roughly 0.4 eV. Noticeably, the first band feature **A** is weakly positive ($+0.3 \times 10^{-40}$ c.g.s.) in the length gauge and weakly negative (-0.5 $\times$ 10^{-40} c.g.s.) in the velocity gauge at the ADC(3)/d-aug-cc-pVDZ level of theory. This can be attributed to basis set incompleteness. **A** arises from the first excited state which is again characterized by n-Rydberg character, as all other computed higher-lying states of norcamphor as well. The second band of the experimental ECD spectrum, **B**, is caused by the second vertical excited state and again aligns excellently with the experimental reference. The sharply positive third band, **C**, arises from a convolution of the third and fourth excited states with vibrational fine structure appearing in the experimental spectrum. **D** arises from convolutions of the fifth to seventh excited states which are hard to separate.

At the ADC(2)/d-aug-cc-pVDZ level, **A**, **B** and **C** are consistently reproduced as those at ADC(3) level. A shift of −0.14 eV is applied to agree with experiment. **B** and **C** are both red-shifted by ∼1.0 eV with rotatory strengths roughly half as those calculated at ADC(3) level. **D** is not reproduced at the ADC(2) level from the lowest ten electronic excited states.

(1*R*)-fenchone. Lastly we turn to (1*R*)-fenchone, which is a constitutional isomer of (1R)-camphor. Not surprisingly, all computed excited states of fenchone correspond again to transitions from lone-pair oxygen n-orbitals to Rydberg orbitals. The first band feature **A** is a dark state in the UV/VIS spectrum as was the case

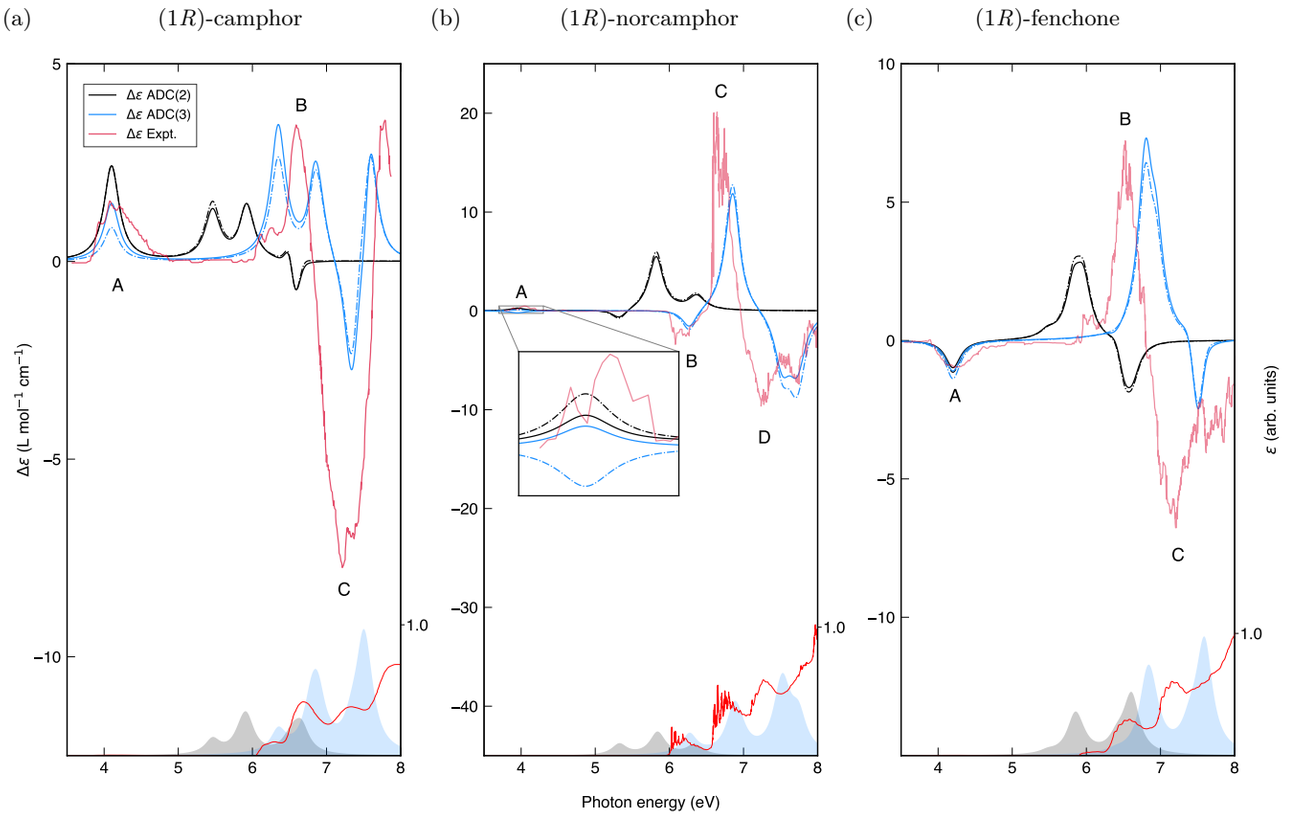

FIG. 6. ECD (top) and UV/VIS (bottom) spectra in the length (solid) and velocity (dashed) gauges of camphor (a), norcamphor (b) and fenchone (c) computed at ADC(3) and ADC(2) levels of theory using the d-aug-cc-pVDZ basis set for norcamphor and aug-cc-pVDZ for camphor and fenchone, the ten lowest states are used to plot the spectra. The ADC(3) spectra have been shifted, -0.32 eV, -0.40 eV and -0.18 eV for camphor, norcamphor and fenchone, respectively and the ADC(2) spectra have been shifted, -0.08 eV, -0.14 eV and +0.04 eV for camphor, norcamphor and fenchone, respectively. Experimental data (red line) are taken from Ref. 96, the UV/VIS experimental line has been normalized to fit calculated values.

for (1R)-camphor, yet becomes visible in the ECD spectrum, again arising from the energetically lowest excited state which is in good agreement with experiment. The second band structure **B** appears again as a vibrationally resolved peak with a slightly red-shifted shoulder, as was the case for camphor. At ADC(3) level it arises from a convolution of the second to fifth excited states which are further blue-shifted by $\sim$ 0.4 eV from experiment. The Lorentzian broadened spectral amplitude is in excellent agreement with experiment. **C** arises from a convolution of the eighth excitation and upwards.

At ADC(2)/aug-cc-pVDZ level, the spectrum is shifted by +0.04 eV to correspond to the first bright state. At this level, **A**, **B** and **C** are consistently reproduced as those calculated at ADC(3) level. The rotatory strength of **A** is within 10% of those at ADC(3) level. **B** and **C** are red-shifted by $\sim$1.0 eV and the rotatory strengths are roughly half of those obtained at ADC(3) level.

IV. SUMMARY AND CONCLUSIONS

Expressions for the calculation of rotatory strength in the length and velocity gauges have been implemented for the algebraic diagrammatic constructions scheme for the polarization propagator up to third order. The accuracy of the simulated ECD spectra using the ADC(2) and ADC(3) schemes has assessed by comparison to the corresponding coupled cluster schemes CC2, CCSD and, for the smaller systems, also CC3. For that objective, the gas phase ECD spectra of the *R*-enantiomers of methyloxirane, methylthiirane, dimethyloxirane, dimethylthiirane, hydrogenperoxid, hydrogendisulfide, camphor, norcamphor and fenchone have been computed. Furthermore, addressing the spectra of molecules in solution, the water spectrum of epinephrine was evaluated using ADC(2) in combination with the polarizable continuum model.

A strong basis set dependence of the computed rotatory strengths has been observed, in particular with respect to the inclusion of diffuse orbital functions. How-

ever, this owes to the n-Rydberg excitation character of all transitions studied here, and can be expected to be less prominent when other chiral organic molecules involving less diffuse $n-\pi^*$ and $\pi-\pi^*$ electronic transitions are investigated.

Not surprisingly, ADC(2) yields rotatory strengths and ECD spectra very similar to those obtained at the CC2 level. ADC(3) produces spectra similar in quality to CCSD which are both comparable to CC3. ADC(3) spectra are in better agreement with the experimental ones for the larger systems studied here, i.e. camphor, norcamphor and fenchone, than for the smaller molecules. For the purpose of assigning an ECD spectrum to one specific enantiomer, ADC(2) and ADC(3) are clearly sufficiently accurate. Together they represent an excellent complementary toolbox for the simulation of ECD spectra which holds promise that the same will also apply for other chiro-optical properties that will be the subject of future studies.

An important aspect in the simulation of experimental ECD spectra of medium-sized to large molecules is the influence of molecular environments, as has been shown for the solution spectrum of epinephrine where the application of PCM shifted the simulated spectrum. Within the ADC framework, further different solvation models are available, for example frozen density embedding,[100,101] effective fragment potentials[102] or polarizable embedding.[103,104] The suitability of these environment models in combination with ADC for the simulation of ECD spectra will be investigated in the future.

SUPPLEMENTARY MATERIAL

Optimized geometries, excitation energies, rotatory and oscillator strengths of all excited states computed are provided in the supplementary material. The impact of the oxygen-oxygen bond contraction on the rotatory strengths of H_2O_2 computed at ADC(3) level as well as the basis set impact on excitation energies and rotatory strengths of methyloxirane are also included.

ACKNOWLEDGMENTS

We acknowledge financial support from the Marie Skłodowska-Curie European Training Network COSINE, grant no. 765739 and VR 2018-4343. Computational resources from the Swedish National Infrastructure for Computing (SNIC), are also acknowledged.

DATA AVAILABILITY

The data that supports the findings of this study are available within the article and its supplementary material.

[1]L. D. Barron, *Molecular Light Scattering and Optical Activity* (Cambridge University Press, 2004).
[2]N. J. Greenfield, Nature Protocols **1**, 2876 (2006), arXiv:NIHMS150003.
[3]C. Bertucci, M. Pistolozzi, and A. De Simone, Analytical and Bioanalytical Chemistry **398**, 155 (2010).
[4]S. Allenmark, Chirality **15**, 409 (2003).
[5]G. Bringmann, K.-P. Gulden, B. Holger, J. Fleischhauer, B. Kramer, and E. Zobel, Tetrahedron **49**, 3305 (1993).
[6]E. Botek and B. Champagne, The Journal of Chemical Physics **127**, 204101 (2007).
[7]P. Polavarapu, Molecular Physics **91**, 551 (1997).
[8]T. Bondo Pedersen and A. E. Hansen, Chemical Physics Letters **246**, 1 (1995).
[9]A. E. Hansen and K. L. Bak, Journal of Physical Chemistry A **104**, 11362 (2000).
[10]P. Bouř, The Journal of Physical Chemistry A **103**, 5099 (1999).
[11]J. R. Cheeseman, M. J. Frisch, F. J. Devlin, and P. J. Stephens, The Journal of Physical Chemistry A **104**, 1039 (2000).
[12]P. J. Stephens, F. J. Devlin, J. R. Cheeseman, and M. J. Frisch, The Journal of Physical Chemistry A **105**, 5356 (2001).
[13]P. Stephens, D. McCann, J. Cheeseman, and M. Frisch, Chirality **17**, S52 (2005).
[14]M. Pecul and K. Ruud, in *Advances in Quantum Chemistry*, Vol. 50 (2005) pp. 185–212.
[15]P. Norman, D. M. Bishop, H. J. A. Jensen, and J. Oddershede, The Journal of Chemical Physics **123**, 194103 (2005).
[16]B. Helmich-Paris, The Journal of Chemical Physics **150**, 174121 (2019).
[17]T. D. Kowalczyk, M. L. Abrams, and T. D. Crawford, The Journal of Physical Chemistry A **110**, 7649 (2006).
[18]T. D. Crawford, M. C. Tam, and M. L. Abrams, Molecular Physics **105**, 2607 (2007).
[19]T. B. Pedersen, H. Koch, and K. Ruud, The Journal of Chemical Physics **110**, 2883 (1999).
[20]K. Ruud, P. J. Stephens, F. J. Devlin, P. R. Taylor, J. R. Cheeseman, and M. J. Frisch, Chemical Physics Letters **373**, 606 (2003).
[21]M. C. Tam, N. J. Russ, and T. D. Crawford, The Journal of Chemical Physics **121**, 3550 (2004).
[22]J. Kongsted, A. E. Hansen, T. B. Pedersen, A. Osted, K. V. Mikkelsen, and O. Christiansen, Chemical Physics Letters **391**, 259 (2004).
[23]J. Schirmer, Physical Review A **26**, 2395 (1982).
[24]S. Knippenberg, D. R. Rehn, M. Wormit, J. H. Starcke, I. L. Rusakova, A. B. Trofimov, and A. Dreuw, The Journal of Chemical Physics **136**, 064107 (2012).
[25]D. R. Rehn, A. Dreuw, and P. Norman, Journal of Chemical Theory and Computation **13**, 5552 (2017).
[26]T. Fransson, D. R. Rehn, A. Dreuw, and P. Norman, The Journal of Chemical Physics **146**, 094301 (2017).
[27]M. Scheurer, T. Fransson, P. Norman, A. Dreuw, and D. R. Rehn, The Journal of Chemical Physics **153**, 074112 (2020).
[28]H. E. Morita, T. S. Kodama, and T. Tanaka, Chirality **18**, 783 (2006).
[29]P. Bouř, J. McCann, and H. Wieser, The Journal of Physical Chemistry A **102**, 102 (1998).
[30]E. Debie, L. Jaspers, P. Bultinck, W. Herrebout, and B. V. D. Veken, Chemical Physics Letters **450**, 426 (2008).
[31]F. J. Devlin and P. J. Stephens, Journal of the American Chemical Society **116**, 5003 (1994).
[32]F. J. Devlin, P. J. Stephens, J. R. Cheeseman, and M. J. Frisch, The Journal of Physical Chemistry A **101**, 6322 (1997).
[33]H. F. BROWN, D. DIFRANCESCO, and S. J. NOBLE, Nature **280**, 235 (1979).
[34]D. Kirkpatrick, J. Yang, and M. Trehy, Journal of Liquid Chromatography & Related Technologies **40**, 556 (2017).
[35]K. Ruud, T. Helgaker, P. Jørgensen, and K. L. Bak, Chemical Physics Letters **223**, 12 (1994).

[36]K. Ruud, T. Helgaker, R. Kobayashi, P. Jo/rgensen, K. L. Bak, and H. J. A. Jensen, The Journal of Chemical Physics **100**, 8178 (1994).
[37]A. M. Lee, N. C. Handy, and S. M. Colwell, The Journal of Chemical Physics **103**, 10095 (1995).
[38]T. Helgaker, P. J. Wilson, R. D. Amos, and N. C. Handy, Journal of Chemical Physics **113**, 2983 (2000).
[39]T. Helgaker, K. Ruud, K. L. Bak, P. Jørgensen, and J. Olsen, Faraday Discuss. **99**, 165 (1994).
[40]J. Gauss, K. Ruud, and T. Helgaker, The Journal of Chemical Physics **105**, 2804 (1996).
[41]K. L. Bak, P. Jørgensen, T. Helgaker, K. Ruud, and H. Jo/rgen Aa. Jensen, The Journal of Chemical Physics **100**, 6620 (1994).
[42]K. L. Bak, A. E. Hansen, K. Ruud, T. Helgaker, J. Olsen, and P. Jørgensen, Theoretica Chimica Acta **90**, 441 (1995).
[43]A. E. Hansen and T. D. Bouman (2007) pp. 545–644.
[44]T. B. Pedersen and H. Koch, Chemical Physics Letters **293**, 251 (1998).
[45]C. D. Pemmaraju, F. D. Vila, J. J. Kas, S. A. Sato, J. J. Rehr, K. Yabana, and D. Prendergast, Computer Physics Communications **226**, 30 (2018), arXiv:1710.08573.
[46]A. Taghizadeh and T. G. Pedersen, Physical Review B **97**, 205432 (2018), arXiv:1804.04869.
[47]T. B. Pedersen, H. Koch, L. Boman, and A. M. Sánchez de Merás, Chemical Physics Letters **393**, 319 (2004).
[48]S. Grimme, S. Peyerimhoff, S. Bartram, F. Vögtle, A. Breest, and J. Hormes, Chemical Physics Letters **213**, 32 (1993).
[49]J. Autschbach, T. Ziegler, S. J. A. van Gisbergen, and E. J. Baerends, The Journal of Chemical Physics **116**, 6930 (2002).
[50]L. Rosenfeld, Zeitschrift für Physik **52**, 161 (1929).
[51]R. A. Harris, The Journal of Chemical Physics **50**, 3947 (1969).
[52]W. Moffitt, The Journal of Chemical Physics **25**, 467 (1956).
[53]H. A. Bethe and E. E. Salpeter, *Quantum Mechanics of One- and Two-Electron Atoms* (Springer US, Boston, MA, 1977).
[54]J. Schirmer and A. B. Trofimov, The Journal of Chemical Physics **120**, 11449 (2004).
[55]A. B. Trofimov, I. L. Krivdina, J. Weller, and J. Schirmer, Chemical Physics **329**, 1 (2006).
[56]P. H. P. Harbach, M. Wormit, and A. Dreuw, The Journal of Chemical Physics **141**, 064113 (2014).
[57]A. Dreuw and M. Wormit, Wiley Interdisciplinary Reviews: Computational Molecular Science **5**, 82 (2015).
[58]J. Schirmer, *Many-Body Methods for Atoms, Molecules and Clusters*, Lecture Notes in Chemistry, Vol. 94 (Springer International Publishing, Cham, 2018) p. 332.
[59]A. Jiemchooroj and P. Norman, The Journal of Chemical Physics **126**, 134102 (2007).
[60]Y. Shao, Z. Gan, E. Epifanovsky, A. T. Gilbert, M. Wormit, J. Kussmann, A. W. Lange, A. Behn, J. Deng, X. Feng, D. Ghosh, M. Goldey, P. R. Horn, L. D. Jacobson, I. Kaliman, R. Z. Khaliullin, T. Kuś, A. Landau, J. Liu, E. I. Proynov, Y. M. Rhee, R. M. Richard, M. A. Rohrdanz, R. P. Steele, E. J. Sundstrom, H. L. Woodcock, P. M. Zimmerman, D. Zuev, B. Albrecht, E. Alguire, B. Austin, G. J. O. Beran, Y. A. Bernard, E. Berquist, K. Brandhorst, K. B. Bravaya, S. T. Brown, D. Casanova, C.-M. Chang, Y. Chen, S. H. Chien, K. D. Closser, D. L. Crittenden, M. Diedenhofen, R. A. DiStasio, H. Do, A. D. Dutoi, R. G. Edgar, S. Fatehi, L. Fusti-Molnar, A. Ghysels, A. Golubeva-Zadorozhnaya, J. Gomes, M. W. Hanson-Heine, P. H. Harbach, A. W. Hauser, E. G. Hohenstein, Z. C. Holden, T.-C. Jagau, H. Ji, B. Kaduk, K. Khistyaev, J. Kim, J. Kim, R. A. King, P. Klunzinger, D. Kosenkov, T. Kowalczyk, C. M. Krauter, K. U. Lao, A. D. Laurent, K. V. Lawler, S. V. Levchenko, C. Y. Lin, F. Liu, E. Livshits, R. C. Lochan, A. Luenser, P. Manohar, S. F. Manzer, S.-P. Mao, N. Mardirossian, A. V. Marenich, S. A. Maurer, N. J. Mayhall, E. Neuscamman, C. M. Oana, R. Olivares-Amaya, D. P. O'Neill, J. A. Parkhill, T. M. Perrine, R. Peverati, A. Prociuk, D. R. Rehn, E. Rosta, N. J. Russ, S. M. Sharada, S. Sharma, D. W. Small, A. Sodt, T. Stein, D. Stück, Y.-C. Su, A. J. Thom, T. Tsuchimochi, V. Vanovschi, L. Vogt, O. Vydrov, T. Wang, M. A. Watson, J. Wenzel, A. White, C. F. Williams, J. Yang, S. Yeganeh, S. R. Yost, Z.-Q. You, I. Y. Zhang, X. Zhang, Y. Zhao, B. R. Brooks, G. K. Chan, D. M. Chipman, C. J. Cramer, W. A. Goddard, M. S. Gordon, W. J. Hehre, A. Klamt, H. F. Schaefer, M. W. Schmidt, C. D. Sherrill, D. G. Truhlar, A. Warshel, X. Xu, A. Aspuru-Guzik, R. Baer, A. T. Bell, N. A. Besley, J.-D. Chai, A. Dreuw, B. D. Dunietz, T. R. Furlani, S. R. Gwaltney, C.-P. Hsu, Y. Jung, J. Kong, D. S. Lambrecht, W. Liang, C. Ochsenfeld, V. A. Rassolov, L. V. Slipchenko, J. E. Subotnik, T. Van Voorhis, J. M. Herbert, A. I. Krylov, P. M. Gill, and M. Head-Gordon, Molecular Physics **113**, 184 (2015).
[61]K. Aidas, C. Angeli, K. L. Bak, V. Bakken, R. Bast, L. Boman, O. Christiansen, R. Cimiraglia, S. Coriani, P. Dahle, E. K. Dalskov, U. Ekström, T. Enevoldsen, J. J. Eriksen, P. Ettenhuber, B. Fernández, L. Ferrighi, H. Fliegl, L. Frediani, K. Hald, A. Halkier, C. Hättig, H. Heiberg, T. Helgaker, A. C. Hennum, H. Hettema, E. Hjertenæs, S. Høst, I.-M. Høyvik, M. F. Iozzi, B. Jansík, H. J. Aa. Jensen, D. Jonsson, P. Jørgensen, J. Kauczor, S. Kirpekar, T. Kjærgaard, W. Klopper, S. Knecht, R. Kobayashi, H. Koch, J. Kongsted, A. Krapp, K. Kristensen, A. Ligabue, O. B. Lutnæs, J. I. Melo, K. V. Mikkelsen, R. H. Myhre, C. Neiss, C. B. Nielsen, P. Norman, J. Olsen, J. M. H. Olsen, A. Osted, M. J. Packer, F. Pawlowski, T. B. Pedersen, P. F. Provasi, S. Reine, Z. Rinkevicius, T. A. Ruden, K. Ruud, V. V. Rybkin, P. Sałek, C. C. M. Samson, A. S. de Merás, T. Saue, S. P. A. Sauer, B. Schimmelpfennig, K. Sneskov, A. H. Steindal, K. O. Sylvester-Hvid, P. R. Taylor, A. M. Teale, E. I. Tellgren, D. P. Tew, A. J. Thorvaldsen, L. Thøgersen, O. Vahtras, M. A. Watson, D. J. D. Wilson, M. Ziolkowski, and H. Ågren, WIREs Comput. Mol. Sci. **4**, 269 (2014).
[62]D. E. Woon and T. H. Dunning, The Journal of Chemical Physics **103**, 4572 (1995).
[63]R. A. Kendall, T. H. Dunning, and R. J. Harrison, The Journal of Chemical Physics **96**, 6796 (1992).
[64]R. A. Kendall, T. H. Dunning, and R. J. Harrison, The Journal of Chemical Physics **96**, 6796 (1992).
[65]D. E. Woon and T. H. Dunning, The Journal of Chemical Physics **103**, 4572 (1995).
[66]T. Yanai, D. P. Tew, and N. C. Handy, Chemical Physics Letters **393**, 51 (2004).
[67]A. Breest, P. Ochmann, F. Pulm, K. Gödderz, M. Carnell, and J. Hormes, Molecular Physics **82**, 539 (1994).
[68]M. Carnell, S. Peyerimhoff, A. Breest, K. Gödderz, P. Ochmann, and J. Hormes, Chemical Physics Letters **180**, 477 (1991).
[69]J. Kongsted, T. B. Pedersen, M. Strange, A. Osted, A. E. Hansen, K. V. Mikkelsen, F. Pawlowski, P. Jørgensen, and C. Hättig, Chemical Physics Letters **401**, 385 (2005).
[70]A. Rizzo and O. Vahtras, The Journal of Chemical Physics **134**, 244109 (2011).
[71]A. Rizzo, N. Lin, and K. Ruud, The Journal of Chemical Physics **128**, 164312 (2008).
[72]T. D. Crawford, M. C. Tam, and M. L. Abrams, Journal of Physical Chemistry A **111**, 12057 (2007).
[73]F. Lipparini, F. Egidi, C. Cappelli, and V. Barone, Journal of Chemical Theory and Computation **9**, 1880 (2013).
[74]P. Mukhopadhyay, G. Zuber, M.-R. Goldsmith, P. Wipf, and D. N. Beratan, ChemPhysChem **7**, 2483 (2006).
[75]J. Šebestík and P. Bouř, The Journal of Physical Chemistry Letters **2**, 498 (2011).
[76]F. Egidi, I. Carnimeo, and C. Cappelli, Optical Materials Express **5**, 196 (2015).
[77]K. B. Wiberg, Y.-g. Wang, P. H. Vaccaro, J. R. Cheeseman, G. Trucks, and M. J. Frisch, The Journal of Physical Chemistry A **108**, 32 (2004).
[78]H. Dothe, M. A. Lowe, and J. S. Alper, The Journal of Physical Chemistry **92**, 6246 (1988).
[79]P. K. Bose, L. D. Barron, and P. L. Polavarapu, Chemical Physics Letters **155**, 423 (1989).
[80]D. Shcherbin and K. Ruud, Chemical Physics **349**, 234 (2008).

[81]T. Miyahara, J.-y. Hasegawa, and H. Nakatsuji, Bulletin of the Chemical Society of Japan **82**, 1215 (2009).
[82]M. Carnell and S. Peyerimhoff, Chemical Physics **183**, 37 (1994).
[83]J. Neugebauer, E. Jan Baerends, M. Nooijen, and J. Autschbach, The Journal of Chemical Physics **122**, 234305 (2005).
[84]A. Rauk, Journal of the American Chemical Society **106**, 6517 (1984).
[85]T.-K. Ha and W. Cencek, Chemical Physics Letters **182**, 519 (1991).
[86]C. Diedrich and S. Grimme, The Journal of Physical Chemistry A **107**, 2524 (2003).
[87]D. H. Szulczewski and W.-h. Hong (1978) pp. 193–229.
[88]A. W. Lange and J. M. Herbert, The Journal of Chemical Physics **133**, 244111 (2010).
[89]A. W. Lange and J. M. Herbert, Chemical Physics Letters **509**, 77 (2011).
[90]T. van Mourik, Physical Chemistry Chemical Physics **6**, 2827 (2004).
[91]J. Y. Cassim and J. T. Yang, Biochemistry **8**, 1947 (1969).
[92]T. Yamada, A. Yamamoto, A. Matsunaga, T. Watanabe, and H. Nakazawa, Analytical Sciences **16**, 325 (2000).
[93]J. P. Hennessey and W. Johnson, Analytical Biochemistry **125**, 177 (1982).
[94]Y. J. Venyaminov SY, *Circular Dichroism and the Conformational Analysis of Biomolecules*, edited by G. D. Fasman (Springer US, Boston, MA, 1996).
[95]A. J. Miles, F. Wien, and B. Wallace, Analytical Biochemistry **335**, 338 (2004).
[96]F. Pulm, J. Schramm, J. Hormes, S. Grimme, and S. D. Peyerimhoff, Chemical Physics **224**, 143 (1997).
[97]M. Stener, D. Di Tommaso, G. Fronzoni, P. Decleva, and I. Powis, The Journal of Chemical Physics **124**, 024326 (2006).
[98]J. Kongsted, B. Mennucci, K. Coutinho, and S. Canuto, Chemical Physics Letters **484**, 185 (2010).
[99]I. Sousa, G. Heerdt, V. Ximenes, A. de Souza, and N. Morgon, Journal of the Brazilian Chemical Society **31**, 613 (2020).
[100]S. Prager, A. Zech, F. Aquilante, A. Dreuw, and T. A. Wesolowski, The Journal of Chemical Physics **144**, 204103 (2016).
[101]S. Prager, A. Zech, T. A. Wesolowski, and A. Dreuw, Journal of Chemical Theory and Computation **13**, 4711 (2017).
[102]R. Sen, A. Dreuw, and S. Faraji, Physical Chemistry Chemical Physics **21**, 3683 (2019).
[103]M. Scheurer, M. F. Herbst, P. Reinholdt, J. M. H. Olsen, A. Dreuw, and J. Kongsted, Journal of Chemical Theory and Computation **14**, 4870 (2018).
[104]A. Marefat Khah, S. Karbalaei Khani, and C. Hättig, Journal of Chemical Theory and Computation **14**, 4640 (2018).

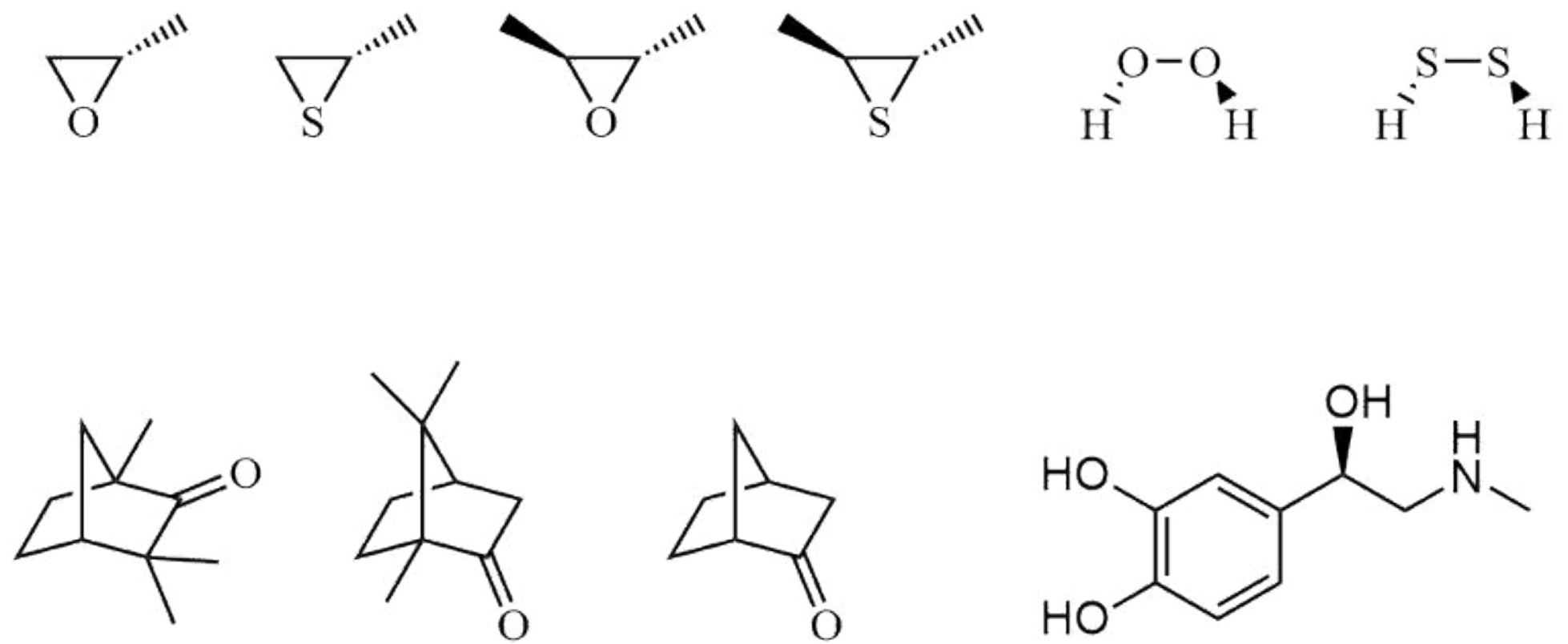
O
S
O
S
O
O
H
H
S
S
H
H
O
O
O
HO
HO
OH
H
N

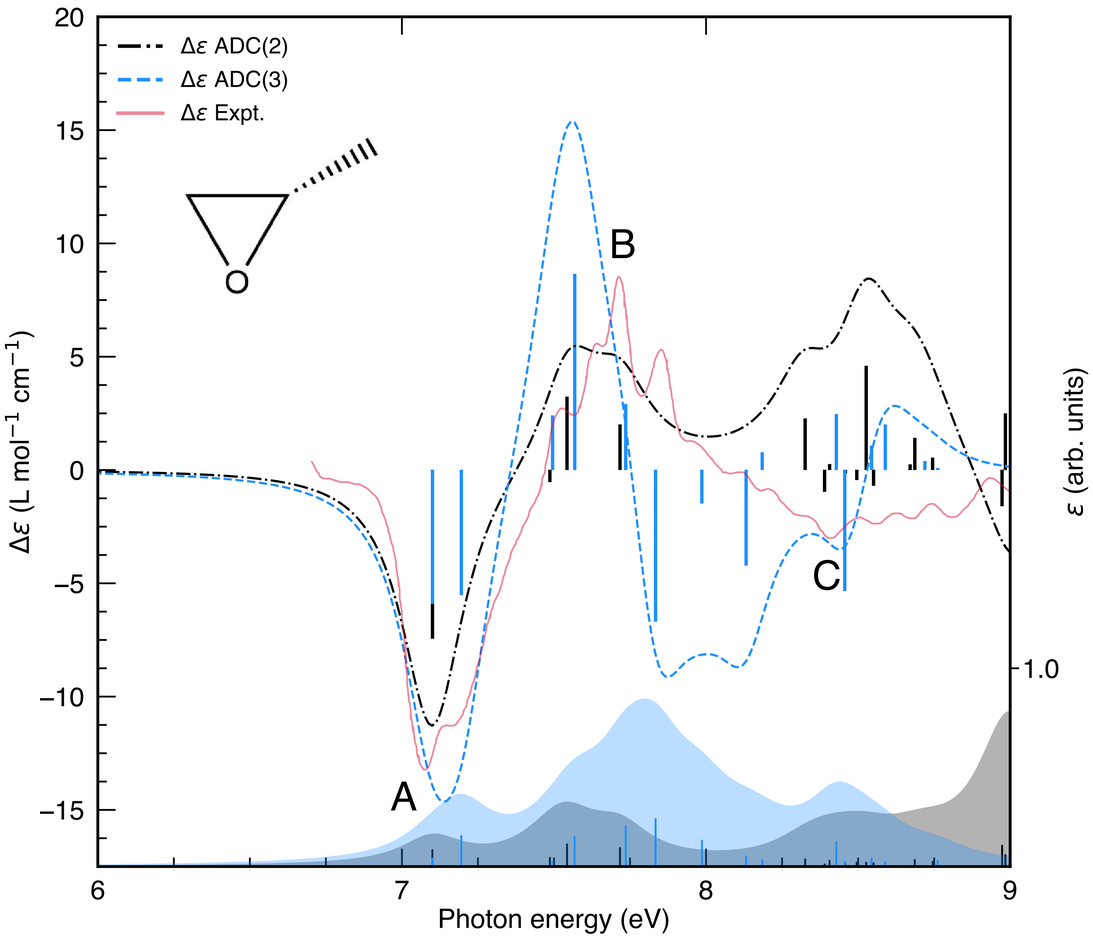
Δε ADC(2)
Δε ADC(3)
Δε Expt.
O
A
B
C
Δε (L mol⁻¹ cm⁻¹)
ε (arb. units)
1.0
Photon energy (eV)

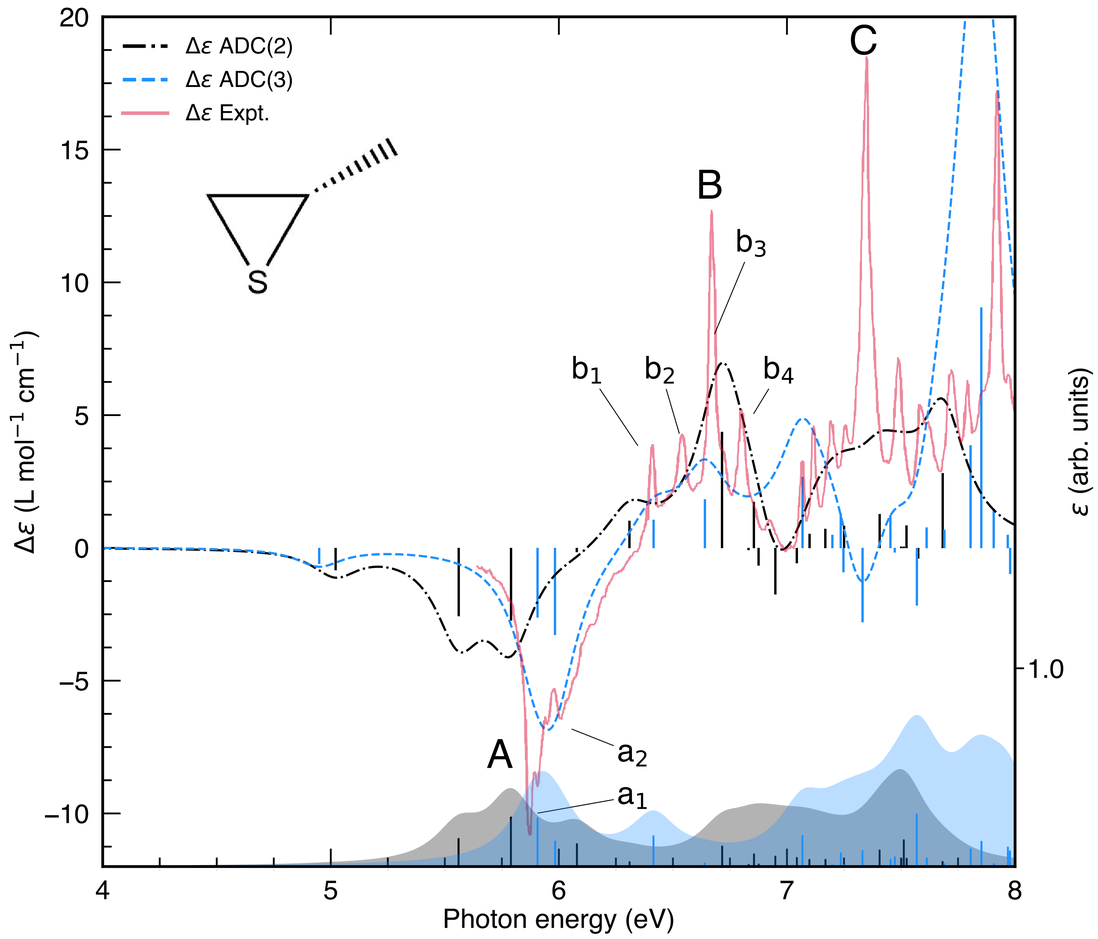
Δε ADC(2)
Δε ADC(3)
Δε Expt.
S
A
B
C
b1
b2
b3
b4
a2
a1
Δε (L mol⁻¹ cm⁻¹)
ε (arb. units)
1.0
Photon energy (eV)

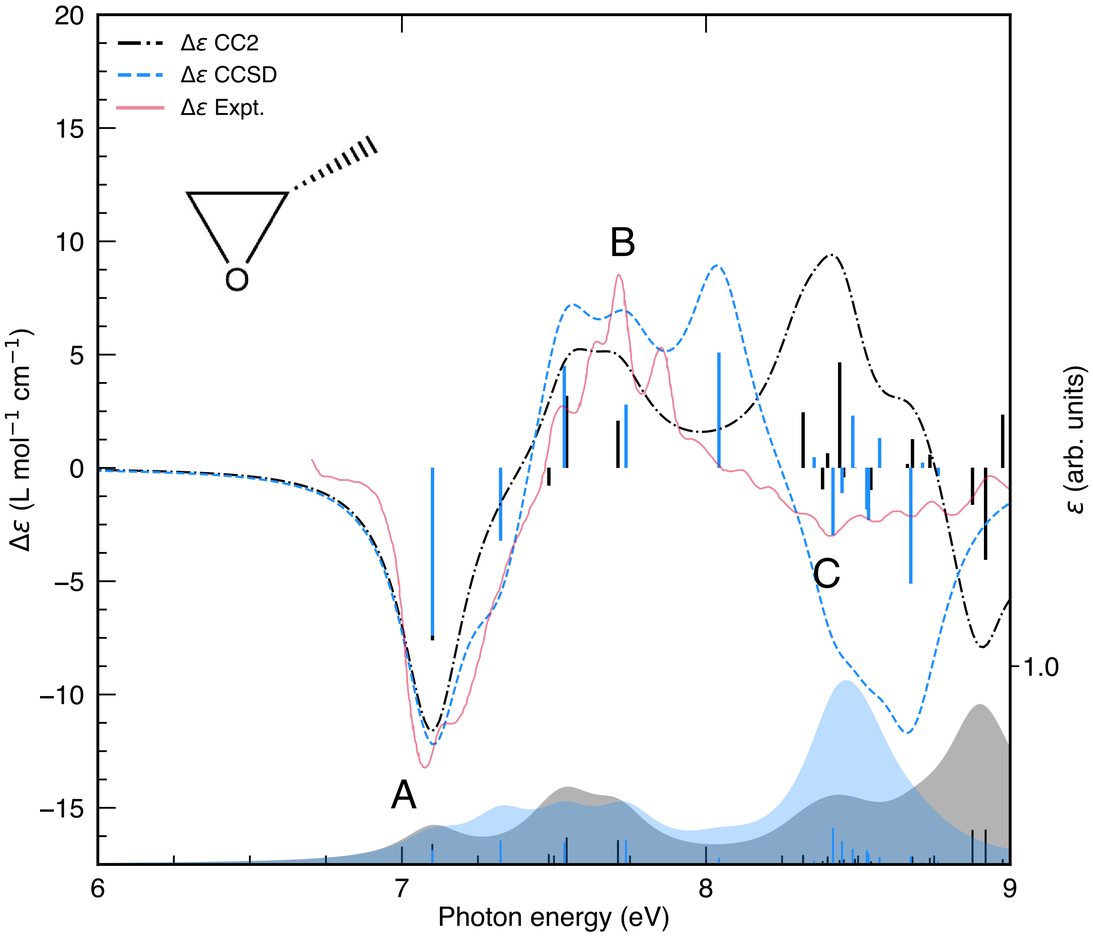
Δε CC2
Δε CCSD
Δε Expt.
O
A
B
C
Δε (L mol⁻¹ cm⁻¹)
ε (arb. units)
1.0
Photon energy (eV)

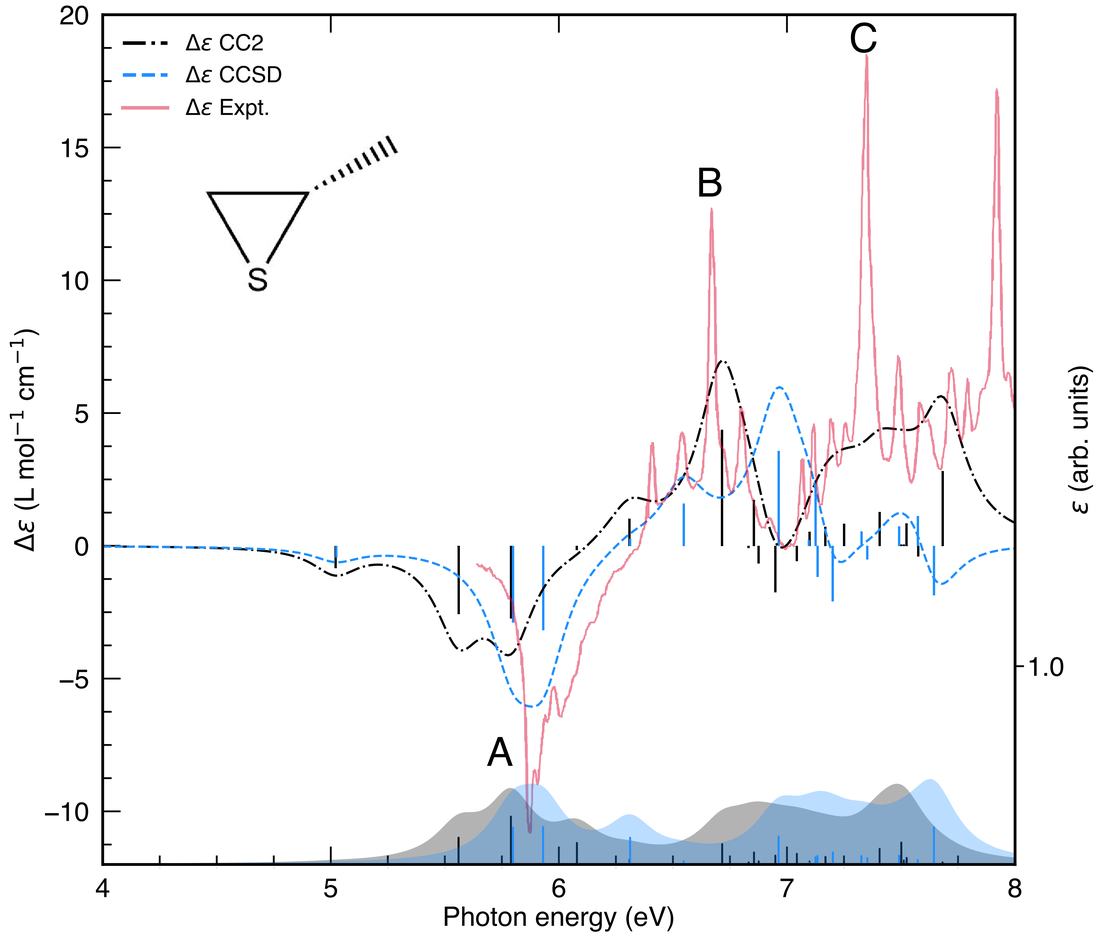
Δε CC2
Δε CCSD
Δε Expt.
S
A
B
C
Δε (L mol⁻¹ cm⁻¹)
ε (arb. units)
1.0
Photon energy (eV)

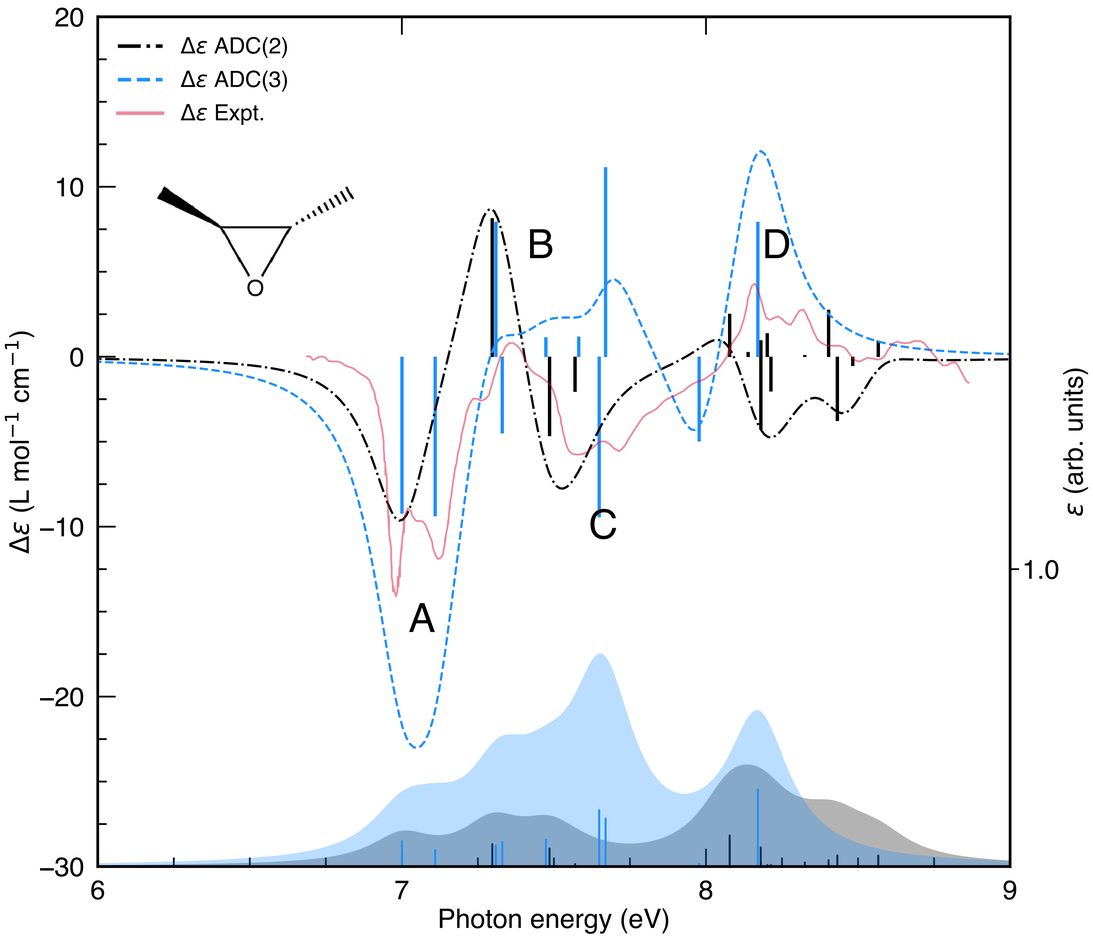
Δε ADC(2)
Δε ADC(3)
Δε Expt.
A
B
C
D
O
Δε (L mol⁻¹ cm⁻¹)
ε (arb. units)
1.0
Photon energy (eV)

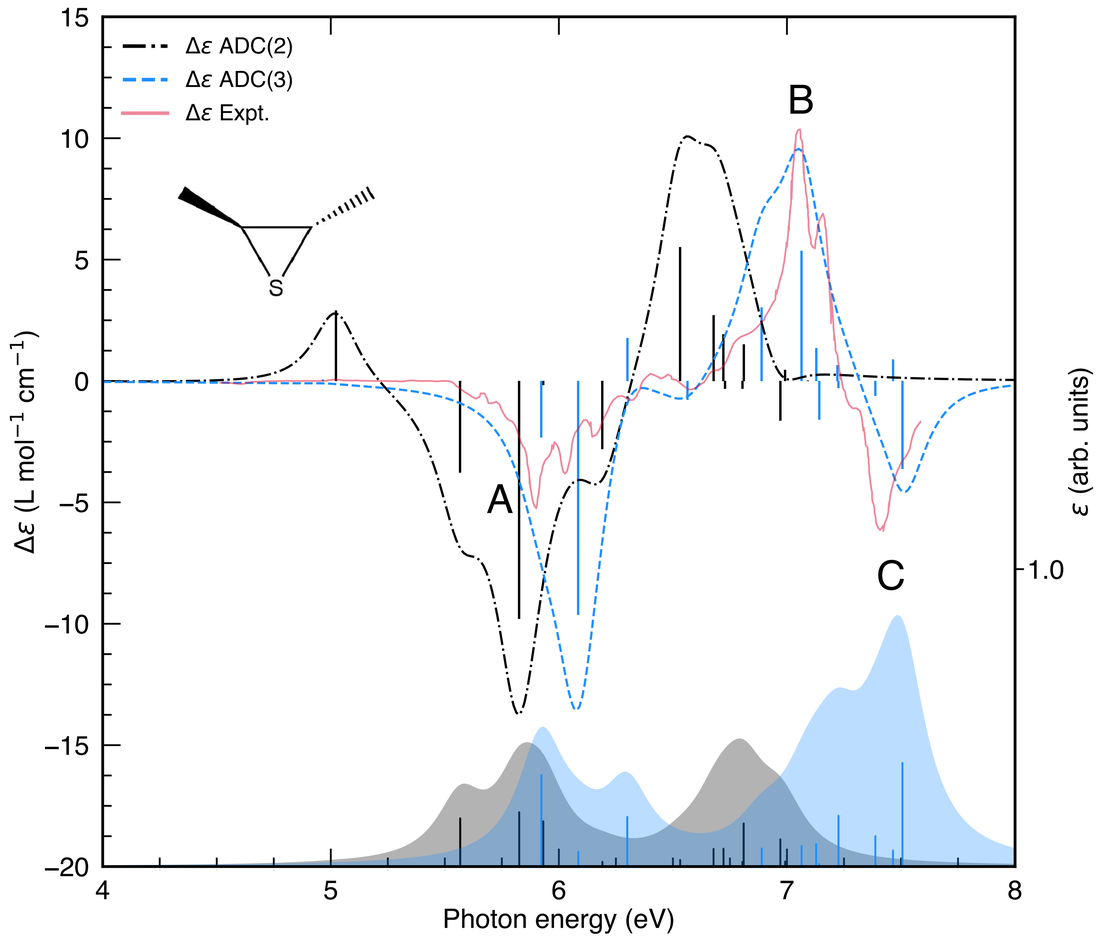
Δε ADC(2)
Δε ADC(3)
Δε Expt.
A
B
C
S
Δε (L mol⁻¹ cm⁻¹)
ε (arb. units)
1.0
Photon energy (eV)

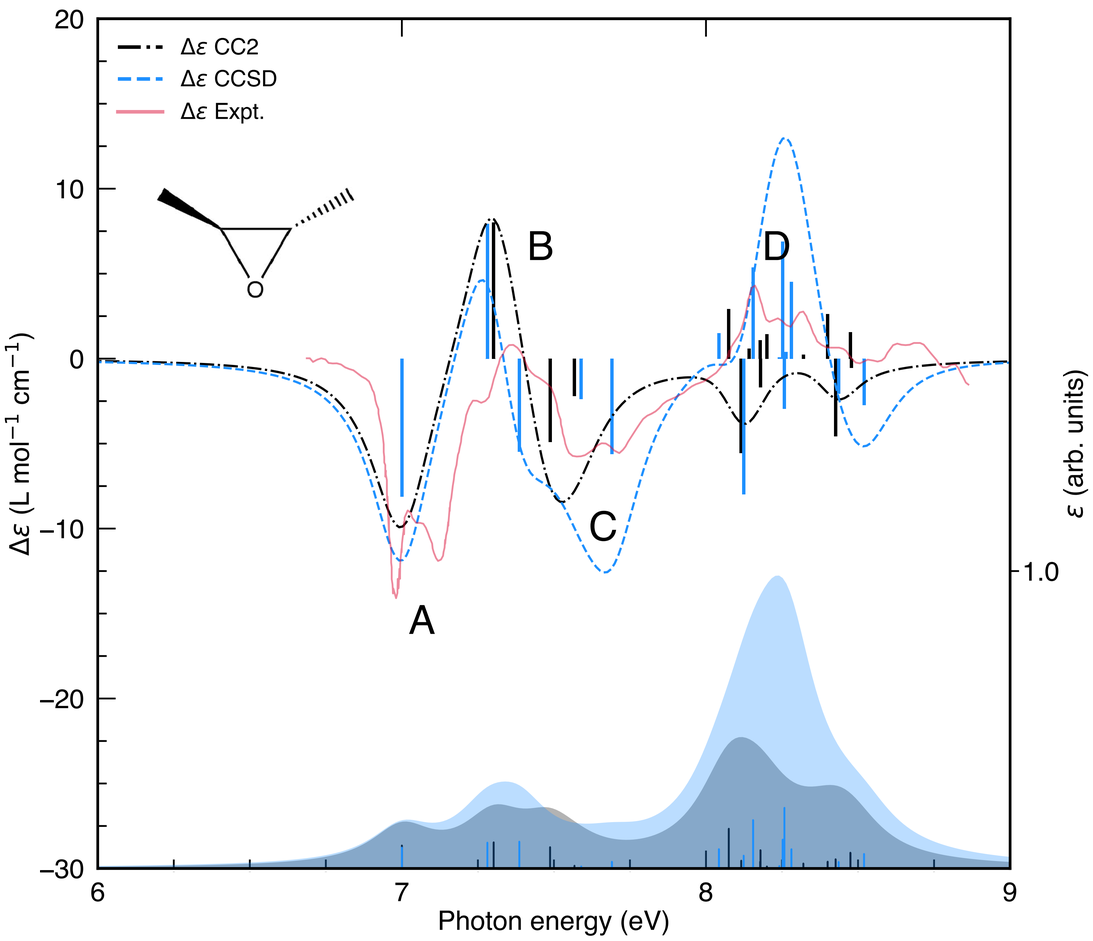
Δε CC2
Δε CCSD
Δε Expt.
A
B
C
D
O
Δε (L mol⁻¹ cm⁻¹)
ε (arb. units)
1.0
Photon energy (eV)

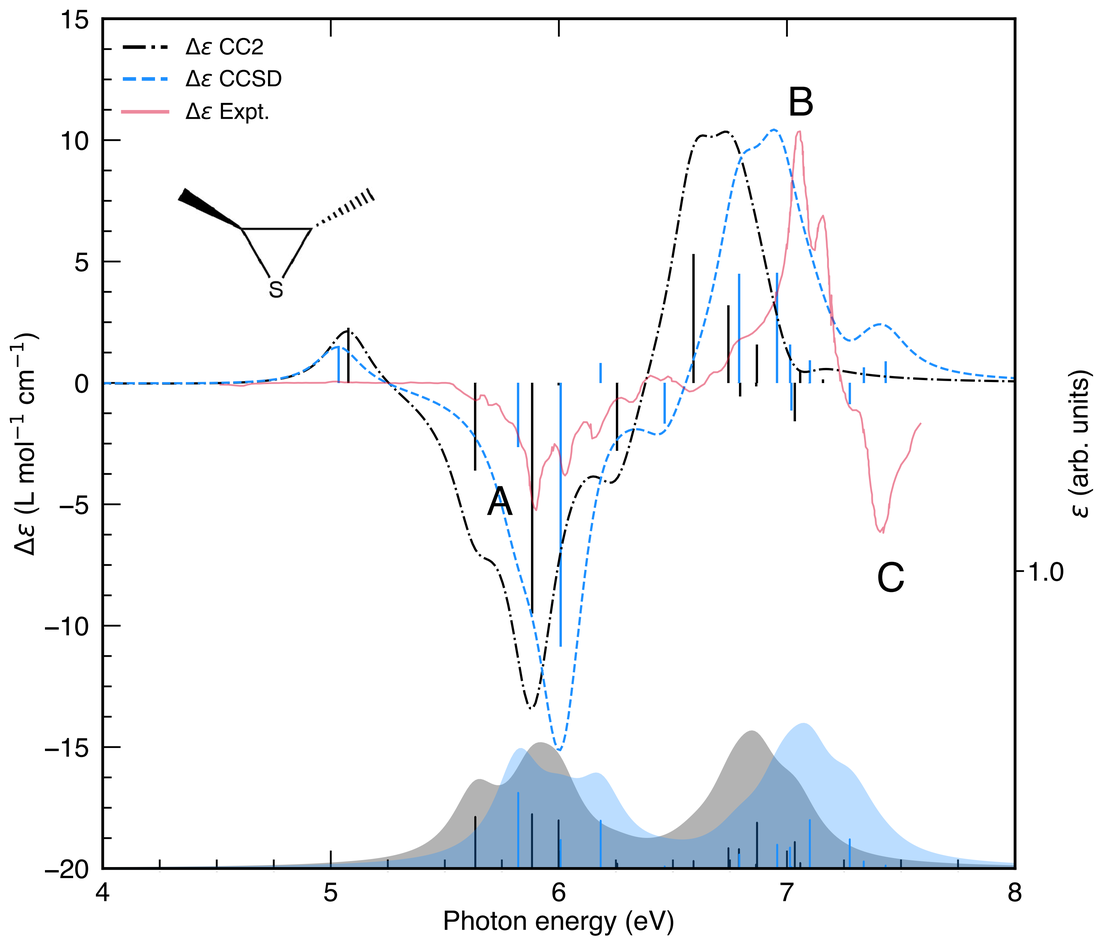
Δε CC2
Δε CCSD
Δε Expt.
A
B
C
S
Δε (L mol⁻¹ cm⁻¹)
ε (arb. units)
1.0
Photon energy (eV)

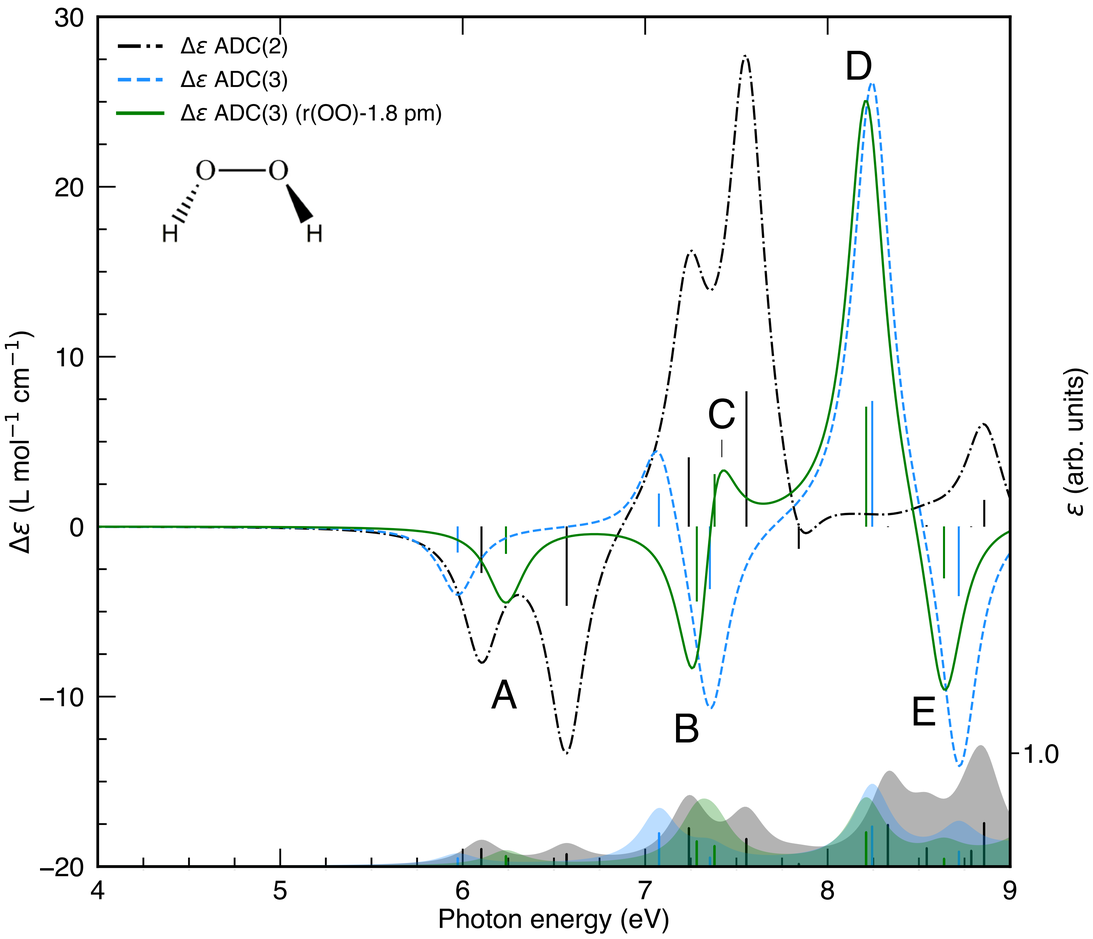
Δε ADC(2)
Δε ADC(3)
Δε ADC(3) (r(OO)-1.8 pm)
O—O
H
H
A
B
C
D
E
Δε (L mol⁻¹ cm⁻¹)
ε (arb. units)
1.0
Photon energy (eV)

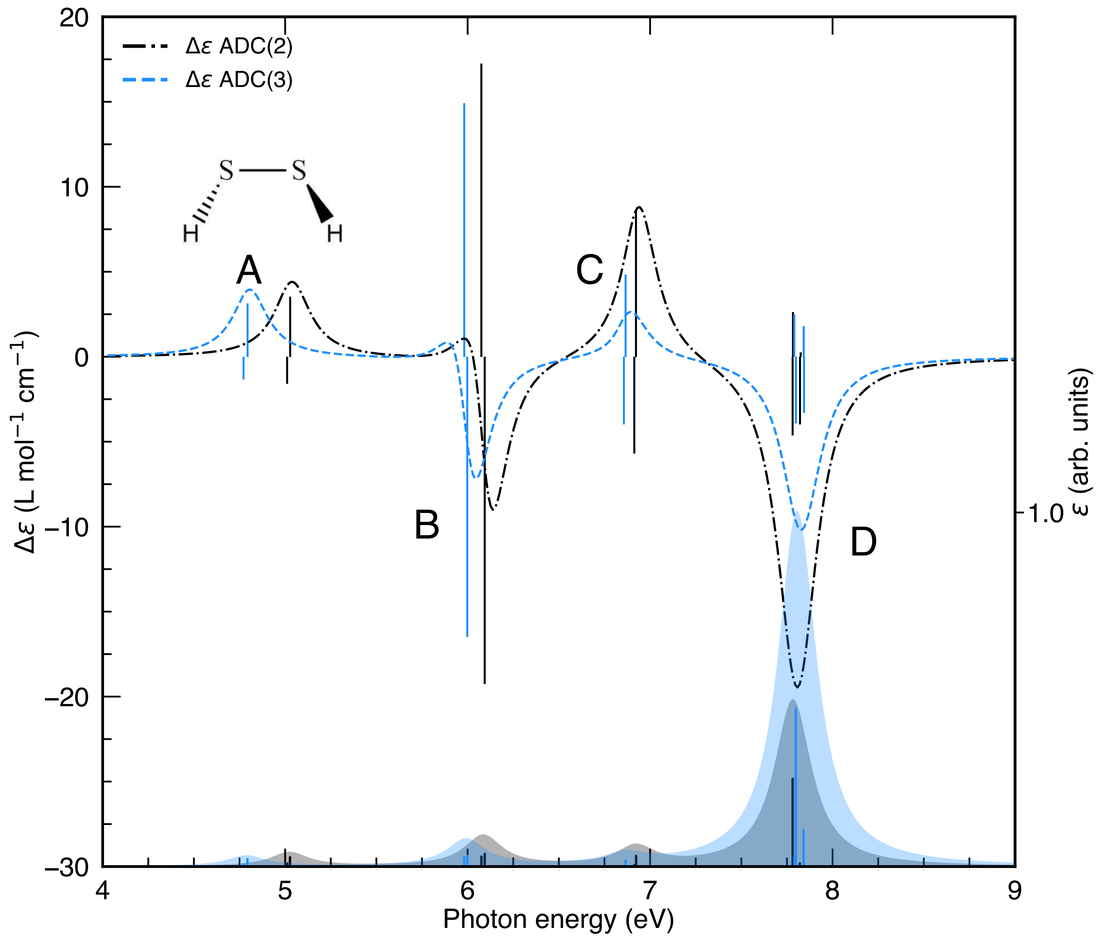
Δε ADC(2)
Δε ADC(3)
S—S
H
H
A
B
C
D
Δε (L mol⁻¹ cm⁻¹)
ε (arb. units)
1.0
Photon energy (eV)

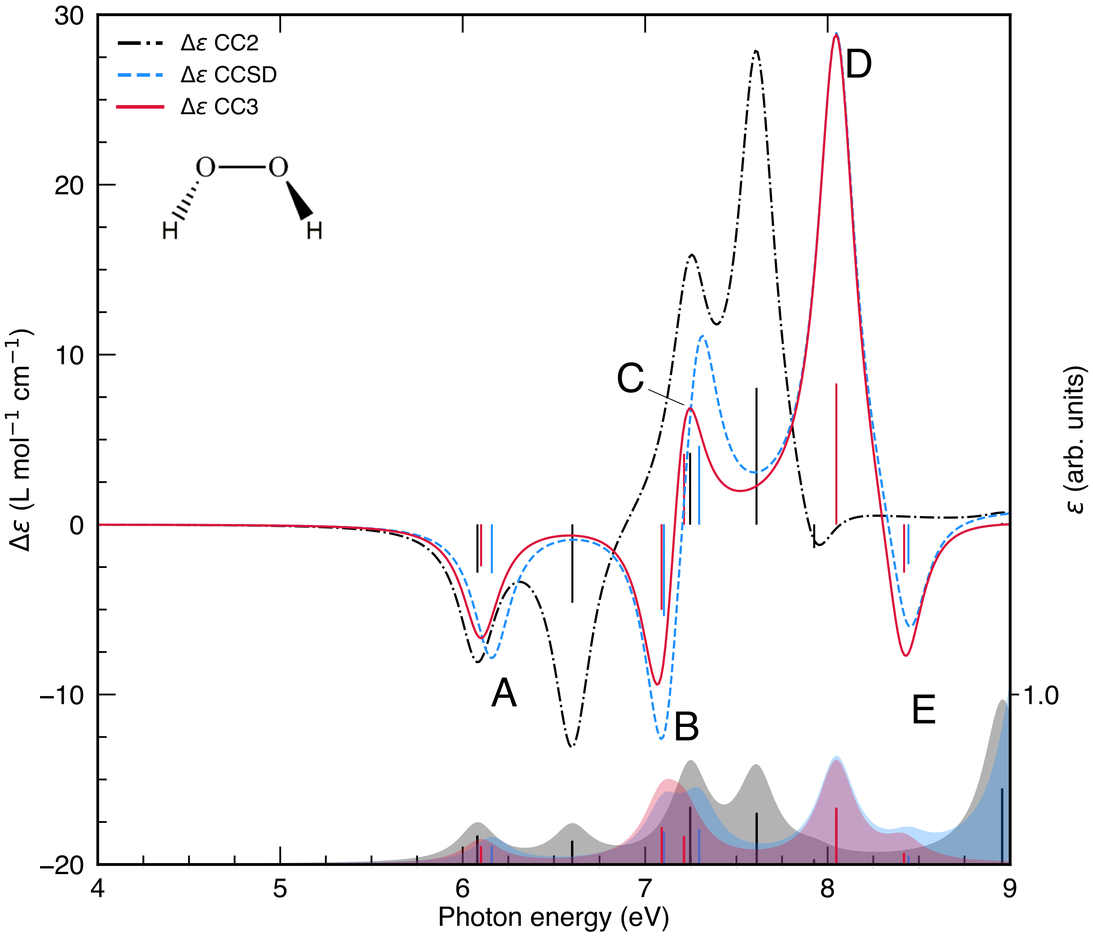
Δε CC2
Δε CCSD
Δε CC3
O—O
H
H
A
B
C
D
E
Δε (L mol⁻¹ cm⁻¹)
ε (arb. units)
1.0
Photon energy (eV)

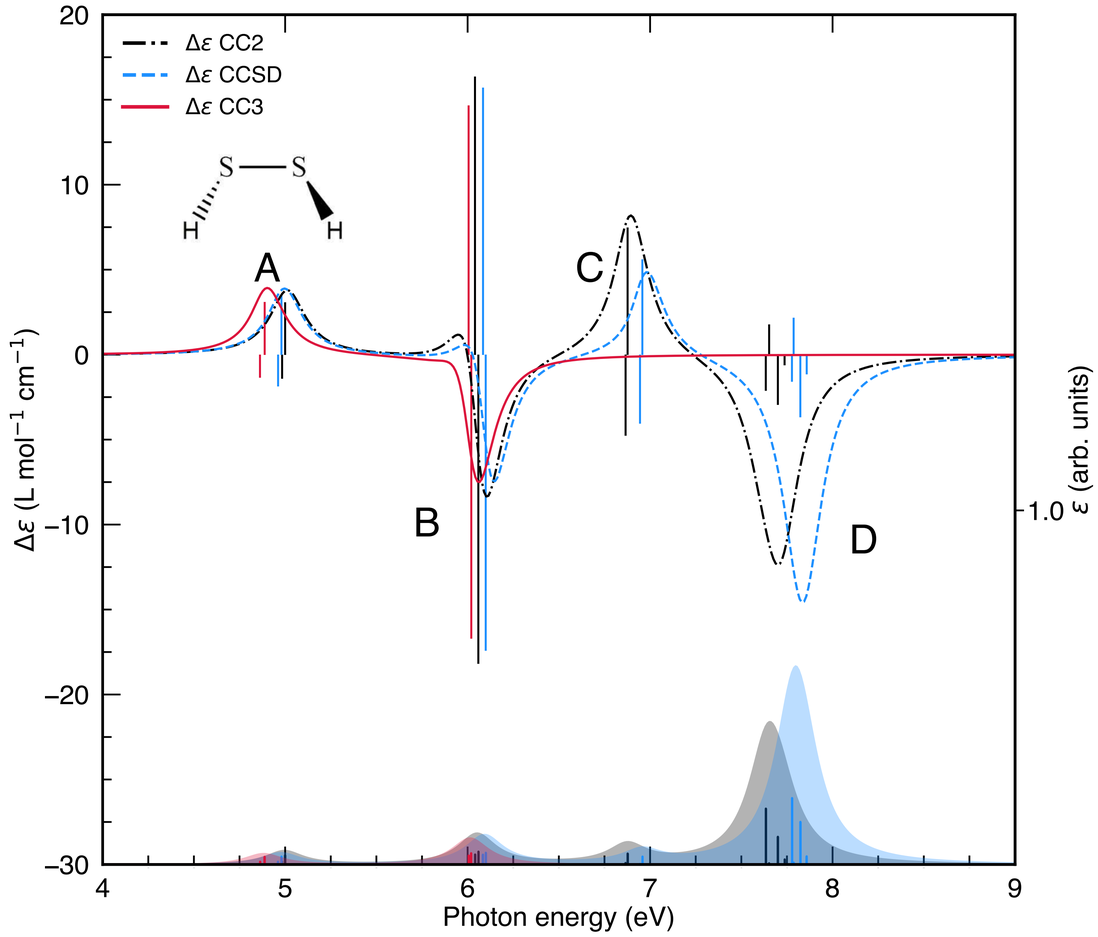
Δε CC2
Δε CCSD
Δε CC3
S—S
H
H
A
B
C
D
Δε (L mol⁻¹ cm⁻¹)
ε (arb. units)
1.0
Photon energy (eV)

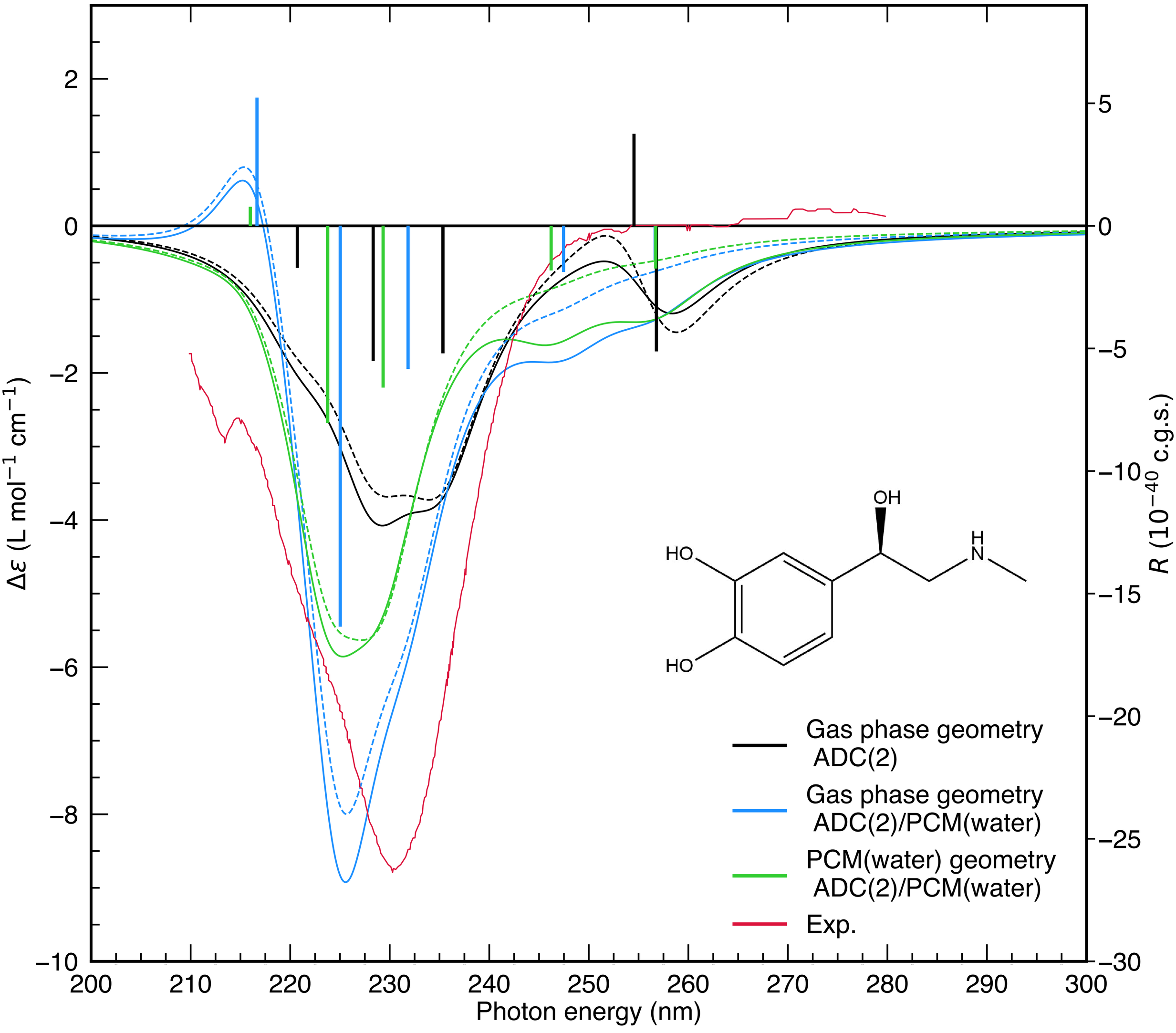
Δε (L mol⁻¹ cm⁻¹)
R (10⁻⁴⁰ c.g.s.)
Photon energy (nm)
200
210
220
230
240
250
260
270
280
290
300
2
0
−2
−4
−6
−8
−10
5
0
−5
−10
−15
−20
−25
−30
OH
HO
HO
H
N
Gas phase geometry
ADC(2)
Gas phase geometry
ADC(2)/PCM(water)
PCM(water) geometry
ADC(2)/PCM(water)
Exp.

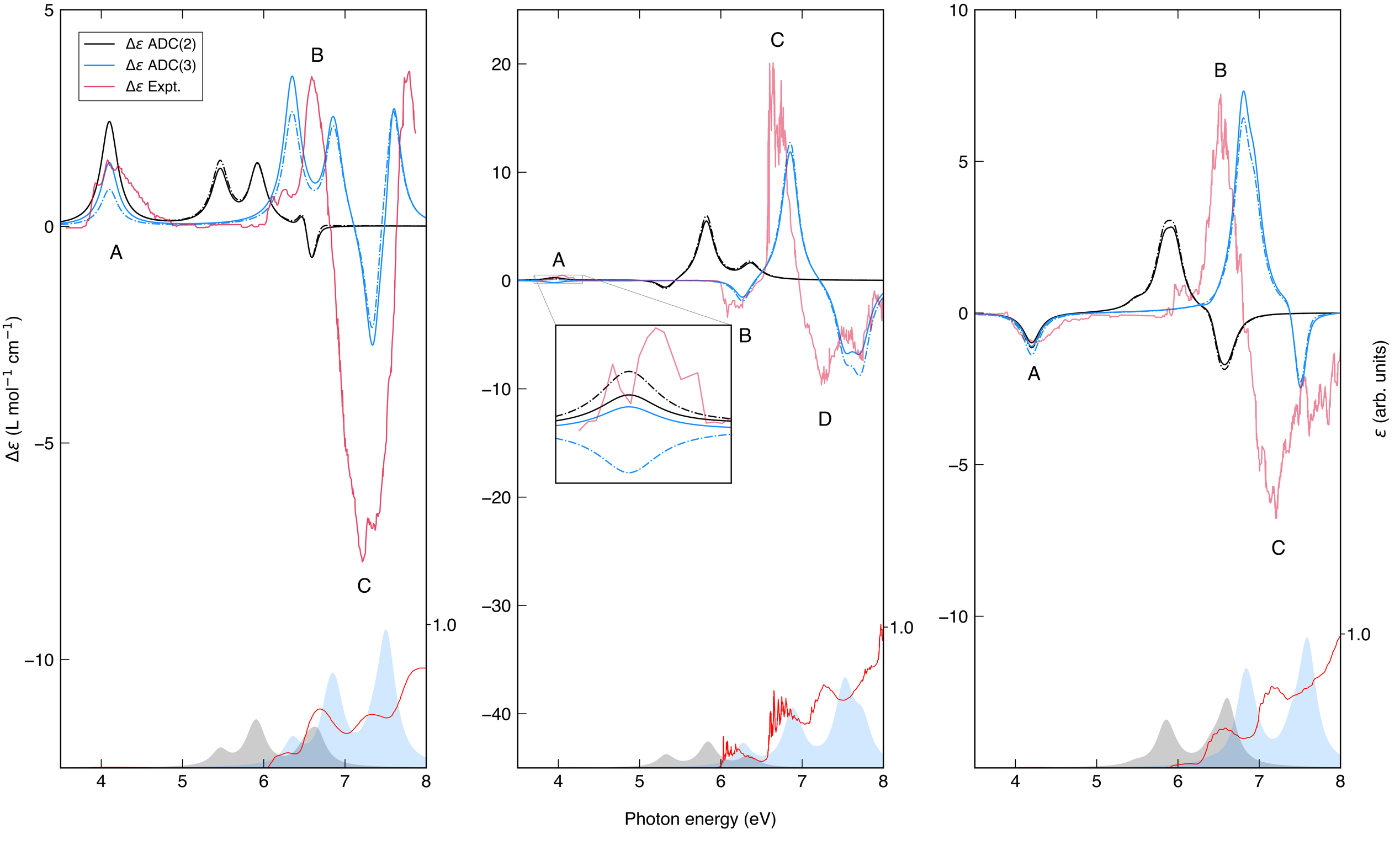
Δε ADC(2)
Δε ADC(3)
Δε Expt.
A
B
C
D
Δε (L mol⁻¹ cm⁻¹)
ε (arb. units)
Photon energy (eV)
1.0